Available online at www.sciencedirect.com

ScienceDirect

Russian Geology and Geophysics 59 (2018) 1161–1181

RUSSIAN GEOLOGY AND GEOPHYSICS

www.elsevier.com/locate/rgg

Paleomagnetism of traps of the Franz Josef Land Archipelago

V.V. Abashev [a,b,*], D.V. Metelkin [b,a], N.E. Mikhaltsov [a,b], V.A. Vernikovsky [a,b], V.Yu. Bragin [a,b]

[a] *A.A. Trofimuk Institute of Petroleum Geology and Geophysics, Siberian Branch of the Russian Academy of Sciences, pr. Akademika Koptyuga 3, Novosibirsk, 630090, Russia*

[b] *Novosibirsk State University, ul. Pirogova 2, Novosibirsk, 630090, Russia*

Received 25 March 2018; accepted 25 April 2018

Abstract

The paper presents results of paleomagnetic studies of traps of the Franz Josef Land (FJL) Archipelago. This area is considered to be part of the Barents Sea Large Igneous Province (LIP) and is usually associated with the Early Cretaceous stage of plume activity, by analogy with other manifestations of late Mesozoic trap magmatism in the High Arctic. Recent isotope-geochemical studies, however, suggest a much longer history of basaltoid magmatism in the FJL area, from Early Jurassic through Early Cretaceous, with three pulses at 190, 155, and ≈125 Ma. Given a significant difference in age, paleomagnetic directions and corresponding virtual geomagnetic poles are supposed to form discrete groups near the Jurassic–Early Cretaceous paleomagnetic poles of Eastern Europe. However, the calculated virtual geomagnetic poles, on the contrary, show a single "cloud" distribution, with its center being shifted to the Early Cretaceous paleomagnetic poles of Siberia. The performed analysis demonstrates that the significant variance is caused mostly by the high-latitude position of the FJL and secular variations of the geomagnetic field during the formation of the traps. Products of the Early Cretaceous magmatism evidently prevail in the data sample. The coincidence of the average paleomagnetic pole of the FJL traps with the Early Cretaceous (145–125 Ma) interval of the apparent polar wander path of Siberia rather than Eastern Europe confirms the hypothesis of the Mesozoic strike-slip activity within the Eurasian continent. This activity might be a natural result of the evolution of the Arctic Ocean.

Keywords: paleomagnetism; Large Igneous Provinces; FJL Archipelago; Arctic

Introduction

Franz Josef Land (FJL) is one of the northernmost Arctic archipelagos consisting of almost two hundred relatively small islands composed mainly of products of intraplate basaltoid magmatism. A thick subhorizontal sequence of lava flow represents a raised fragment of a large igneous province (LIP) formed supposedly in the Late Jurassic–Early Cretaceous. The major part of this LIP covers the entire northern part of the Barents Sea floor up to and including the Svalbard Archipelago, as well as extensive areas lying to the south of Franz Josef Land along Severny Island of Novaya Zemlya in the direction of the Kanin Nos Peninsula (Karyakin and Shipilov, 2009; Shipilov, 2016) and occupies, accordingly, more than a third of the Svalbard plate area, which forms the region's continental shelf structure (Fig. 1), which, apart from the lava flow facies, is strongly represented by sizeable dikes and sills cutting across the Triassic–Jurassic terrigenous complex composed by sandstones, siltstones, and their weakly-cemented analogues (Fig. 1). Thus, the significant amount of effusive rocks and their geochemical signatures leave no doubt about the plume nature of magmatism and the typical trap formation mechanism of the geological structure of the FJL and the adjacent territories (Dobretsov et al., 2013; Ernst, 2014; Karyakin and Shipilov, 2009). Besides the Barents Sea LIP, other manifestations of late Mesozoic basaltoid magmatism are known within the Arctic region including isolated areas, such as: the Sverdrup area (Canadian Arctic Archipelago and adjacent continental shelf) (Evenchick et al., 2015; Jowitt et al., 2014), the East Siberian Sea (the De Long Archipelago and the adjacent continental shelf) (Dobretsov et al., 2013; Filatova and Khain, 2009; Shipilov, 2011) and, finally, the Central Arctic province. Maps of the latter were generated based on the results of marine geophysical studies in combination with dredging and drilling, with the data c covering a vast area comprising the underwater Alpha-Mendeleev Ridge and the adjacent Makarov and Podvodnikov basins up to and including the Chukotka uplift (Kremenetsky et al., 2015; Morozov et al., 2013).

* Corresponding author.
E-mail address: AbashevVV@ipgg.sbras.ru (V.V. Abashev)

1068-7971/$ - see front matter © 2018, V.S. Sobolev IGM, Siberian Branch of the RAS. Published by Elsevier B.V. All rights reserved.
http://dx.doi.org/10.1016/j.rgg.2018.08.010

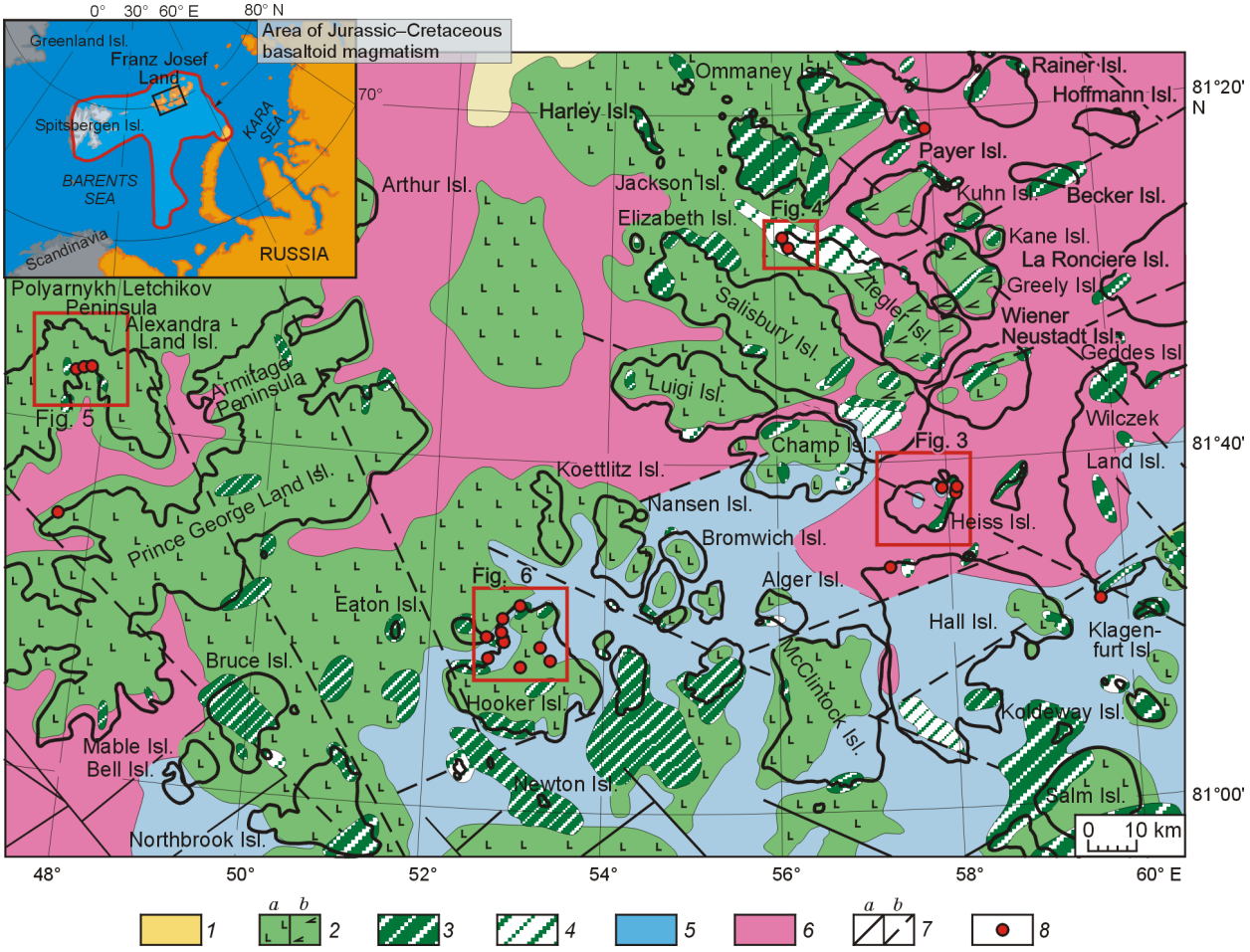

Fig. 1. Schematic geological map of the studied FJL Archipelago area, after (State..., 2006) (revised). The red line in the inset delineates a tentative area of basaltoid magmatism distribution in the Barents Sea LIP, after (Karyakin and Shipilov, 2009). *1*, Oligocene–Pliocene deposits (siltstones, clays); *2–4*, Jurassic (?)–Early Cretaceous trap complex: *2*, tuffs and basalt flows (*a*) and andesibasalts (*b*), *3*, hypabyssal complex (dikes, sills, laccolites) gabbro, gabbro-diorites, gabbro-dolerites, dolerites and monzonites, *4*, vent facies holding extrusive bodies (stocks and nekks) of basalts, andesibasalts; *5*, Jurassic deposits (mudstones, siltstones, sands, sandstones); *6*, Triassic deposits (sands, sandstones, clays, mudstones, siltstones); *7*, faults: established (*a*) and inferred (*b*); *8*, paleomagnetic sampling sites.

The supposed close age of rocks in these areas suggests their association as part of the Jurassic–Cretaceous High Arctic Large Igneous Province (HALIP), formed synchronously with the opening of the Amerasian (Canadian) basin of the Arctic Ocean (Buchan and Ernst, 2006; Dobretsov et al., 2013; Ernst, 2014; Shipilov et al., 2009). Numerous studies have shown that the evolution of this mantle plume is likely associated with the formation of the largest—Siberian—LIP at the turn of the Permian–Triassic, as well as with more ancient manifestations of intraplate magmatism in Northeast Asia (Kuzmin and Yarmolyuk, 2014, 2016; Kuzmin et al., 2010, 2011). The Barents Sea area can thus be regarded as one of the most extensive manifestations of trap magmatism and, given the sufficiently compelling paleomagnetic data, it can be used for absolute plate tectonic reconstructions involving the Arctic terranes in the Mesozoic and for verification of the available geodynamic models of the Arctic basin evolution, primarily the Amerasian (Canadian) basin (Gaina et al., 2014; Koulakov et al., 2013; Laverov et al., 2013; Lawver et al., 2002; Shipilov, 2016; Shipilov and Lobkovskii, 2014; Sokolov et al., 2015; Vernikovsky et al., 2013).

However, reliability of paleomagnetic reconstructions crucially depends on determination of the age of rocks and the time of fixation of the measured magnetization. The episodic behavior, i.e., the formation of a large volume of magmatic rocks in a relatively short period on the geological time scale, is a distinctive feature of LIP magmatism. As is the case with the Siberian LIP, the duration of such pulses is not longer than 15 Ma (Ivanov et al., 2013; Kamo et al., 2003; Reichow et al., 2009), and according to some estimates no more than 1–5 Ma (Kazanskii et al., 2000; Kazansky et al., 2005; Latyshev et al., 2013; Mikhaltsov et al., 2012).

At the same time, a characteristic periodicity of ~ 30 Ma is observed in plume magmatism, which correlates well with large tectonic events in the region, including in the Arctic area, and with global geotectonics (Dobretsov, 2010; Dobretsov et al., 2013). Until recently, the estimated duration of the formation of the FJL traps within the 145–125 Ma interval successfully concorded with the general concept (Corfu et al.,

2013; Grachev, 2001; Ntaflos and Richter, 2003). However, the results of $^{40}Ar/^{39}Ar$ dating (Karyakin and Shipilov, 2009) have corroborated earlier assumptions about the long-term and multistage formation of the LIP (Tarakhovsky et al., 1982).

According to the new data, the age interval of the FJL basaltoid magmatism spans the time period from the Early Jurassic through Early Cretaceous, and includes at least three pulses: Early Jurassic (196–189 Ma), Late Jurassic (160–153 Ma) and the well known and repeatedly substantiated—Early Cretaceous (145–125 Ma) (Dobretsov et al., 2013; Karyakin and Shipilov, 2009; Shipilov and Karyakin, 2010, 2011; Shipilov et al., 2009). The presence of these pulses is supported by the results of studies of the chemical composition of clinopyroxenes and melt inclusions (Dobretsov et al., 2013), which however meets numerous objections drawn from geological facts (Stolbov and Suvorova, 2010). Moreover, available observations suggest that lava flows commonly underlain by sedimentary rocks not older than Early Oxfordian, which rules out the existence of an Early Jurassic magmatism pulse. Besides, there are no signs of any significant hiatuses in the sections of FJL traps, which should exist, given the presumably sporadic nature of magmatism with its activity interrupted by relatively "calm" stages with durations up to 30 Ma. These findings therefore question the reliability of the obtained $^{40}Ar/^{39}Ar$ data.

Paleomagnetic data can be viewed as an additional independent argumentation in favor of the periodic magmatism pattern. Taking into account the assumed significant difference in age and the absence of large-scale late Mesozoic tectonic movements between the Svalbard and the Baltica plates, the virtual geomagnetic poles (VGPs) for the Early Jurassic, Late Jurassic and Early Cretaceous FJL basalts should form discrete groups in close proximity to the respective Eastern European paleomagnetic poles. The first obtained paleomagnetic determinations generally confirmed good prospects for using this approach and even allowed outlining some tectonic effects based on results of the calculated poles position analysis (Mikhaltsov et al., 2016).

Given that quite a large amount of paleomagnetic determinations for traps has thus far been accumulated for a considerable part of the FJL Archipelago, we have attempted to analyze their informative capacity and susceptibility in order to decipher the Barents Sea LIP magmatism evolution, with an aim to provide an independent substantiation of the early stages of magmatism, and consequently, of a possibility of reconstructing the Mesozoic tectonic history of the Arctic using the data obtained.

Object of study

Specifically, the object of our study was the magmatic products, mapped as individual subhorizontally occurring lava flows, as well as major dikes, sills or small stocks within the areas of eight islands of the FJL Archipelago (Fig. 1). Based on morphostructural analysis and geophysical data, the FJL uplift is proposed to be differentiated using a distinctly discernible band of negative magnetic anomalies corresponding to the Markham Strait and to be divided into the southwestern and northeastern segments (Fig. 2*a*) (Shipilov, 2016; Shipilov and Karyakin, 2014). A remarkable feature of the magnetic anomalies in both segments is the presence of lengthy sublatitudinal band anomalies, conformably extending along the strike of this boundary, and the gradual weakening of the total intensity of the geomagnetic field and its band structure across this zonation. In the northwestern part of the archipelago, specifically, in the adjacent off-shore area of the continental shelf, the bands are distinctly visible with the anomalies intensity reaching 300 nT or more; in the southeastern periphery of the archipelago, in the area of the largest (Hall, Wilczek Land, and Graham Bell) islands, the field is relatively uniform with total intensity not exceeding 100 nT (Fig. 2*a*).

The band pattern of positive magnetic anomalies is to be regarded as an indication to the presence of a series of large dikes intruding the FJL section and representing the magma feeder channels for sills and lava flows prevailing on the northwestern flank of the archipelago, which caps the sections of most islands (Shipilov, 2016; Shipilov and Karyakin, 2014). This interpretation is generally corroborated by our map of lithospheric magnetic anomalies, built on the basis of the accessible EMAG2 global database (Global Earth Magnetic Anomaly Grid) (Fig. 2*b*). The band structure appears less discernible here, but the observed transverse submeridional zoning is more distinctly marked by the magnetic anomalies intensity (Fig. 2*b*). Similar zoning patterns of gravity anomalies, on the one hand, reflect the modern terrain, but, on the other hand, can carry additional information about the region's subsurface structure (Fig. 2*b*, *d*). On the Faye anomaly map (free-air gravity anomaly), the entire northwestern part is characterized by a weak positive values zone (up to ≈70 mGal), which probably indicates the presence of flat-topped plateaus formed by lava capping the hypabyssal intrusions, observable in the magnetic field anomalies. The southeastern flank in the modern structure, on the contrary, is characterized by insignificant negative values of the gravity field from 0 to –30 mGal (Fig. 2*d*). Given that previously this part may have been elevated, lava facies either were not formed here, or denudated. Accordingly, the modern erosion surface is dominated by sedimentary rocks hosting sills and dikes, of which one located on the northwestern tip of Hall island in the vicinity of Cape Wiggins was investigated in this study (Fig. 1). According to the available $^{40}Ar/^{39}Ar$ data, the age of dikes averages 132.3 ± 2.0 Ma (Mikhaltsov et al., 2016). A large subconcordant intrusive body (sill) was also sampled at Wilczek Land Island (Fig. 1). A large sill of gabbro-dolerites whose U–Pb zircon age is 122.7 Ma was reported from the Severnaya well, Graham Bell Island within Triassic sedimentary rocks at a depth 1820–1900 m (Corfu et al., 2013). However, the largest emplacement of dikes and sills on present day erosion level is typical of Heiss Island, where we studied the Ametistovaya dike and two sills (lower and upper) intruding in its sedimentary section, on the northeastern tip of the island (Fig. 3). Ametistovaya dike is the youngest, its

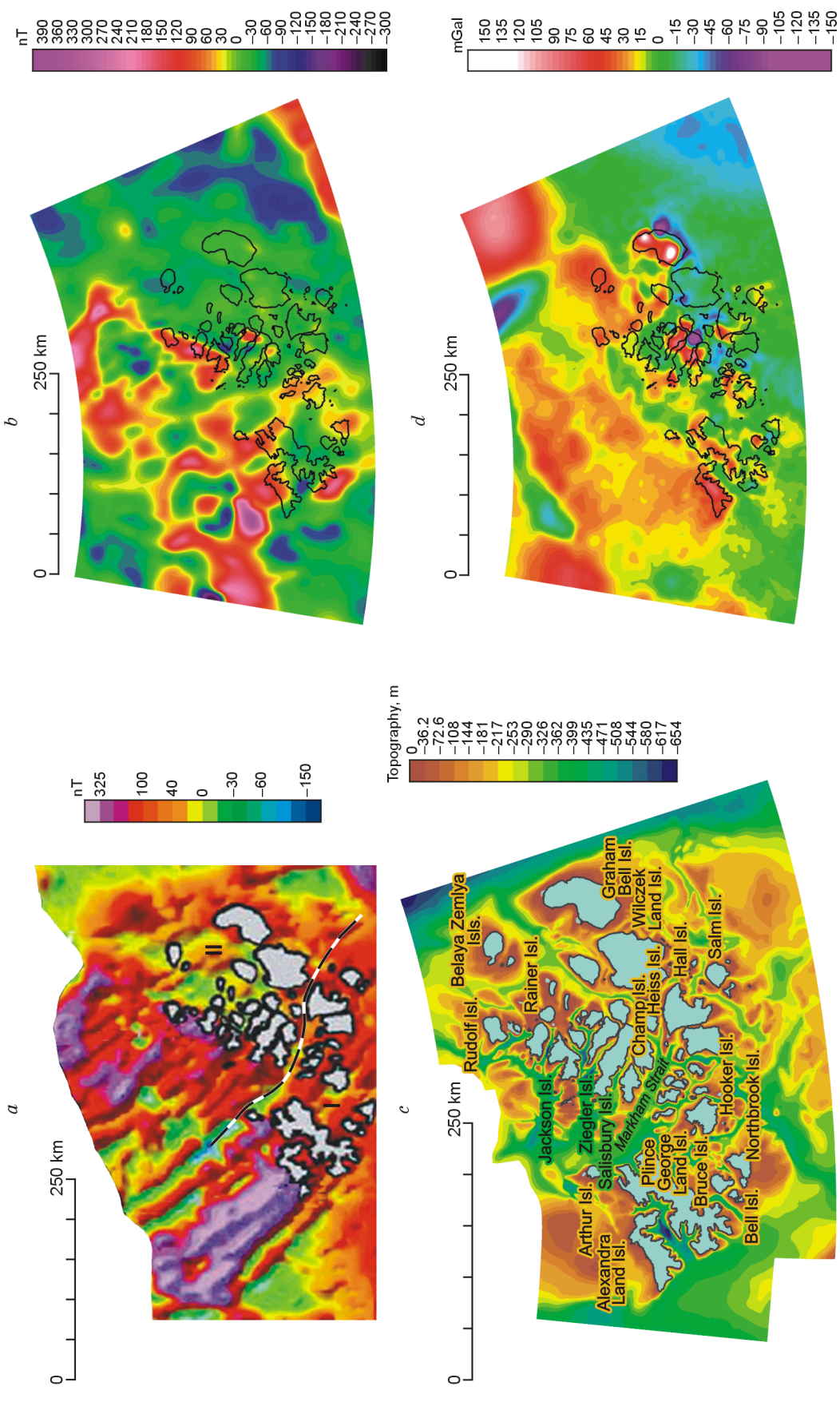

Fig. 2. Map of magnetic field anomalies, after (Minakov et al., 2012; Shipilov, 2016) (*a*); lithospheric magnetic anomalies, according to the EMAG2 Global Database https://www.ngdc.noaa.gov/geomag/emag2.html (*b*); modern terrain from bathymetry data (*c*); Faye free-air gravity anomaly from the DTU15 model (Andersen et al., 2017) (*d*) for FJL area and adjacent continental shelf. *a*: I, southwestern (SW) segment of FJL; II, northeastern (NE) segment of FJL, dashed line shows geophysical boundary between SW–NE segments (see text for explanations).

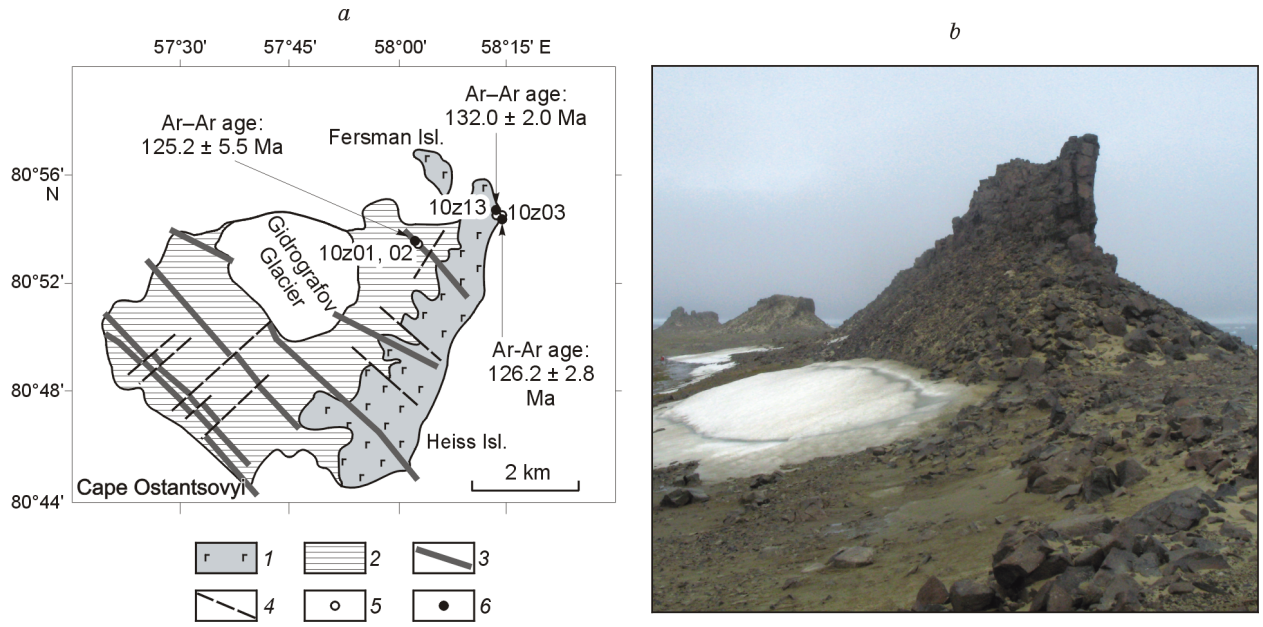

Fig. 3. Geologic aspects of Heiss Island. *a*, Geological framework, after (Shipilov, 2016): *1*, Early Cretaceous lava flows; *2*, Mesozoic sedimentary rocks; *3*, dikes of Early Cretaceous dolerites; *4*, faults; *5*, sites of paleomagnetic sampling with indication of number; *6*, sampling points for geochronological analysis with indication of age determination; *b*, general view of the Ametistovaya dike exposure (sites 10z01, 02, photograph by N. Mikhaltsov).

$^{40}Ar/^{39}Ar$ age is 125.2 ± 2.0 Ma (Shipilov and Karyakin, 2014). According to these authors, it is almost coeval (126.2 ± 2.8 Ma) with the lower sill, and slightly younger than the upper sill whose age is 131.6 ± 2.4 Ma.

The age of the other dikes and the lava flow covering the island is not older than 140 Ma, which is fully consistent with the most manifest Early Cretaceous magmatism pulse. The nature of this pulse or at least the intrusion of dikes is considered by (Shipilov, 2016; Shipilov and Karyakin, 2014) to be reflective of the process of rifting associated with the opening of the Canadian basin. The lava facies, in themselves, corresponding to the Early Cretaceous magmatic episode, are widespread and predominant on the present day erosion level both within the NE and SW segments (Fig. 1) (Piskarev et al., 2009). In the NE segment area, basalt flows were studied only in the outcrops of Ziegler Island, in the vicinity of Cape Brice (Fig. 4). The corresponding Early Cretaceous age of basalts (about 135 Ma) is confirmed by the $^{40}Ar/^{39}Ar$ dating results (Mikhaltsov et al., 2016). Two dikes have been sampled there. According to our preliminary data whose publication is forthcoming, one of these dikes has a tentative age of 126.0 ± 3.5 Ma, while the other may be associated with termination of the Late Jurassic magmatic pulse—148.7 ± 4.2 Ma. Even older Early Jurassic ages are available in the radiological dating summary on age determinations by different methods (K–Ar, Pb–Pb, Sm–Nd) for several sills and lava flows on Rudolf and Jackson Islands, however, these data need refining.

Specifically, the presence of Early Cretaceous, and both—Early and Late—Jurassic episodes of magmatism in modern erosion level distinguish, as suggested by (Shipilov and Karyakin, 2014), the SW segment of the Franz Josef Land Archipelago. Whereas lava facies of all the three pulses are closely spaced in sections without visible signs of long hiatuses. Thus, on Alexandra Land Island (Fig. 5), according to the results of $^{40}Ar/^{39}Ar$ dating from mineral fractions by stepwise heating in the lower flow of amygdaloidal plagioclase basalts with distinctive columnar jointing the obtained values are 189.9 ± 3.1 and 196.5 ± 6.3 Ma (Karyakin and Shipilov, 2009; Shipilov, 2016; Shipilov and Karyakin, 2014). Upwards, in the middle lava flow, characterized by block structure, the plateau age is 156.5 ± 5.3 and 152.6 ± 14.5 Ma (Karyakin and Shipilov, 2009; Shipilov, 2016; Shipilov and Karyakin, 2014). Finally, the upper part of the visible section is formed by a thick basalt flow with giant columnar jointing with the weighted mean age of plagioclase and pyroxene is 135.0 ± 4.0 Ma. This cover caps the section of the island and is most widely distributed throughout the area. Similar ages are reported for the Alexandra Land basalts in (Piskarev et al., 2009). Comparable Jurassic dates 151 ± 11, 192 ± 13, 170 ± 12, 203 ± 14 Ma are available from age determinations for sills intruding Early Mesozoic–Late Paleozoic terrigenous-carbonate deposits, penetrated in the 1300–3200 m depth interval by the Nagurskaya well, located north of the area of works (Fig. 5) (Tarakhovsky et al., 1982).

However, these ages obtained by the bulk rock K–Ar method are unlikely to be reliable. The formation of sills there, as well as on Hall, Heiss, Graham Bell islands in the SE periphery of the archipelago, is more probably connected with the Early Cretaceous episode of magmatism as is confirmed by the U–Pb analysis results for several zircon crystals encountered in these rocks (Corfu et al., 2013). Another manifestation of Early Jurassic magmatism corroborated by the $^{40}Ar/^{39}Ar$ data (189.1 ± 11.4 Ma) is known on Hooker

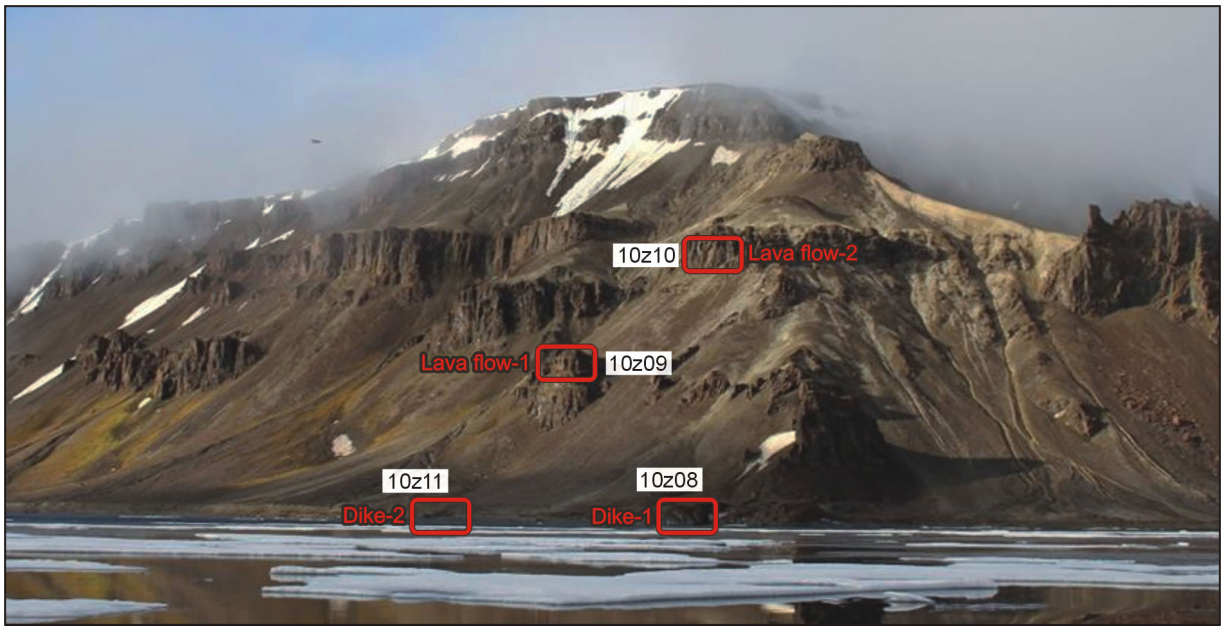

Fig. 4. General view of the northwestern coastline exposures of Ziegler Island. Photograph by Yu. Petrova, borrowed from http://www.rus-arc.ru.

island, at the base of the cliff section in the northern side of Tikhaya Bay, near Cape Sedov (Fig. 6) (Shipilov, 2016; Shipilov and Karyakin, 2014). The authors of this age determination extend it over the entire section forming the Sedov plateau, as far as Albert Markham Cape, however there is a strong possibility that, by analogy with the Alexandra Land Island section, it holds the products of all three magmatic pulses. The dated cover composed of columnar jointed amygdaloid basalts is exposed at an altitude of 100–130 m (Fig. 6*b*). The "higher" horizons of the section, forming the Sedov plateau, were studied in the Tikhaya Bay to the east of Cape Sedov (Fig. 6*c*), as well as those outcropping immediately above the Molchaniya valley and Voronin Glacier. The two lava flows studied on Cape Albert Markham are presumably from the lower part of the section (Fig. 6*g*), however, unambiguous correlation between their exposures here and Tikhaya Bay lavas is problematic.

Magmatic bodies encountered in the section of NW part of the island most likely have intrusive character, i.e., sills, which are composed of vertical columnar jointed well-crystallized medium- to coarse-grained gabbro-dolerites. One of them was samples in several outcrops in the northern side of Tikhaya Bay above Sedov Glacier (Fig. 6*a*), where the sill underlies a thick flow of massive vitreous basalts. The same relationship of crystallized and vitreous rocks can be observed in the cliffs of the Molchaniya valley, and southwards of Cape Medvezhiy. In the latter, the lava flows of black massive vitreous basalts with multidirectional thin-columnar jointing crowns the section forming a rocky outcrop about 120 m in height (Fig. 6*e*). A body of well decrystallized dolerites, greenish-gray in color and more than 15 m thick is observed below the lava flow. The lower boundary of the sill is not exposed, however, directly below it in the slope-wash horizon, there are angular fragments of thin-slabby gray sandstone. This horizon whose thickness totals to 10 m is underlain by yet another dolerite sill with visible thickness about 5 m (Fig. 6*e*).

In the inner part of the island, for the most part covered by glaciers, the sampled section fragments made up by lava facies and extending vertically form individual outcrops of Solnechnaya rock, Pila cliff, and Yuri rock (Fig. 6*f*).

The sampled giant outcrop of Rubini rock on the southernmost side of Tikhaya Bay (Fig. 6*g*), is usually interpreted as a stock whose age from K–Ar determinations is not older than 145 ± 7 Ma (Stolbov, 2005).

A succession of three lava flows is discernible in the studied coastal rocky outcrops on the eastern ending of Scott-Kelty Island located in close proximity to Cape Sedov. The lower and middle lava flows typically have vertical columnar jointing, while the upper flow is differentiated by columnar jointing with multidirectional orientation. All three lava flows have been sampled.

We therefore suggest that the sampled FJL flood basalts relatively uniformly characterize the stages of the Barents Sea LIP magmatic activity inferred from the $^{40}Ar/^{39}Ar$ determinations and form a representative data set of specimens for deciphering its evolution.

Paleomagnetic research methods

The oriented samples were collected with a gasoline powered portable drill or manually. To determine the local magnetic declination, either the solar azimuth or the necessary correction to the data is calculated from the IGRF (International Geomagnetic Reference Field) model. A comparison between the available measurements and model data shows that the local magnetic declination in the studied area of the FJL Archipelago averages 35°.

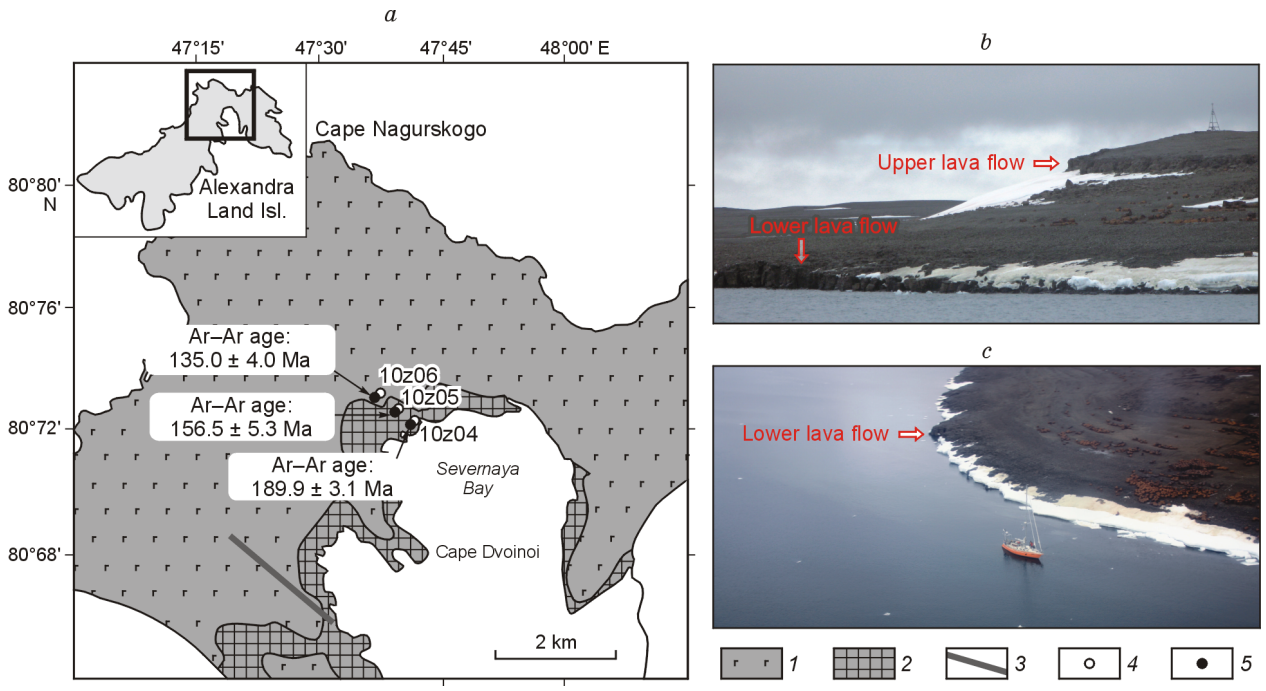

Fig. 5. Geologic aspects of the northeastern part of Alexandra Land Island. *a*, Geological framework, after (Shipilov, 2016; Sklyarov et al., 2016): *1*, Early Cretaceous basalts; 2, Early Jurassic and Late Jurassic basalts, not partitioned; *3*, Early Cretaceous (?) dolerite dike; *4*, paleomagnetic sampling sites with indication of their numbering; 5, sampling sites for geochronological analysis with indication of age determinations (*b*, *c*); general view (from free photo hosting Yandex) of the Severnaya Bay volcanic section.

Laboratory paleomagnetic and rock magnetic experiments were carried out using the equipment of the IPGG SB RAS Geodynamics and paleomagnetism Laboratory and the NSU Laboratory for geodynamics and paleomagnetism of the Central and Eastern Arctic (Novosibirsk). To substantiate the component composition of the natural remanent magnetization (NRM), all samples were subjected to either detailed thermal (*T*) or alternating field (*AF*) demagnetization until their complete demagnetization. The number of demagnetization steps generally varied between 14 and 18. The remanent magnetization vector measurements were performed with a SRM-755 cryogenic magnetometer (2G Enterprises, USA), placed in a space shielded from the external field. The composition of magnetic minerals present in the rock was determined from the results of the study of the temperature dependencies of the magnetic susceptibility $k(T)$ in an inert medium with a MFK1–FA Kappabridge multifunctional meter (AGICO, Czech Republic). Magnetic hysteresis of the specimens was studied with the J-Meter coercivity spectrometer (Kazan, Russia).

The NRM measurements processing was performed with a specialized software (Enkin, 1994), using the component analysis method for magnetization-based screening (Kirschvink, 1980). The position of virtual geomagnetic poles was analyzed using GMAP (Torsvik and Smethurst, 1999). The domain structure of ferromagnetic grains was evaluated from Day plot (Day et al., 1977; Dunlop, 2002).

Results of paleomagnetic studies

Magnetic scalar characteristics. The level of natural remanent magnetization (NRM) of the studied basalts and dolerites is high, slightly varying from 2 to 20 A/m, while the magnetic susceptibility is about 10^{-2} SI units. The relationship between these parameters (Koenigsberger ratio) is above 1, reaching the value of 20. Such parameters are typical of unaltered magmatic rocks and indicate thet the magnetization may have been preserved (Nagata, 1961). Magnetic scalar characteristics of rocks of different ages determined from $^{40}Ar/^{39}Ar$ measurements have exhibited no differences, which indirectly implies a similarity in the mineralogical composition of the carriers of magnetization and the NRM fixation conditions.

Magnetic mineralogy. The studies of temperature dependence of magnetic susceptibility $k(T)$ have shown (Fig. 7) that titanomagnetite and magnetite are the main magnetic minerals in all the analyzed samples. Most common is a high-ferriferous titanomagnetite, with a Curie point (T_C) at 540 °C and above, up to experimentally indistinguishable from T_C of magnetite at 578 °C. However, a low-ferriferous phase is not rare whose T_C can vary from 180 to 400 °C. At the same time, both these minerals can be reported from one sample. When heated, titanomagnetite, especially its low-ferriferous phase, is quickly undergoes irreversible changes, which results in the Curie point shifting towards higher temperatures on the cooling curve. It appears that the currently predominant high-ferruferrous phase is the product of partial single-phase oxidation of

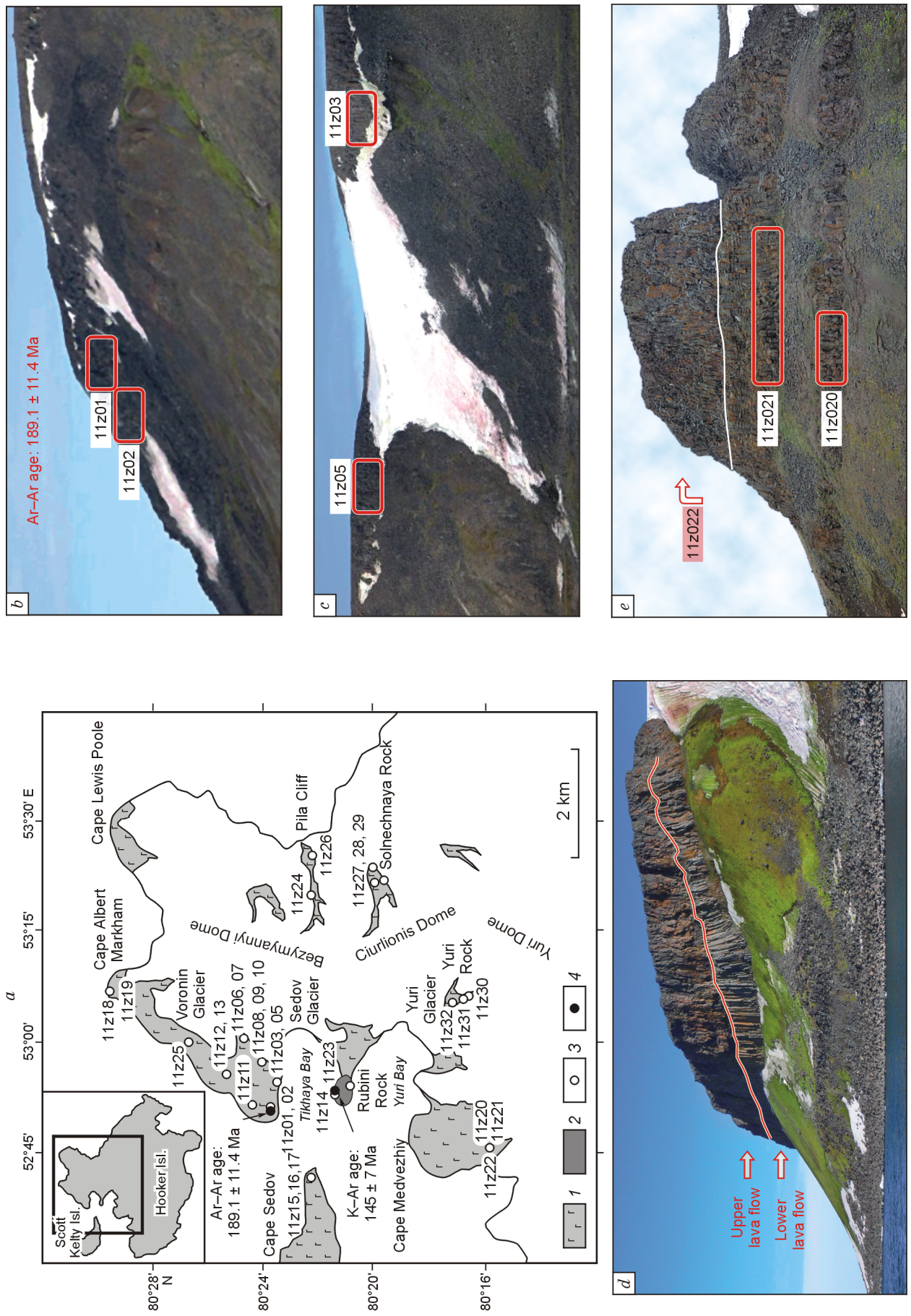

Fig. 6 (*continued on next page*).

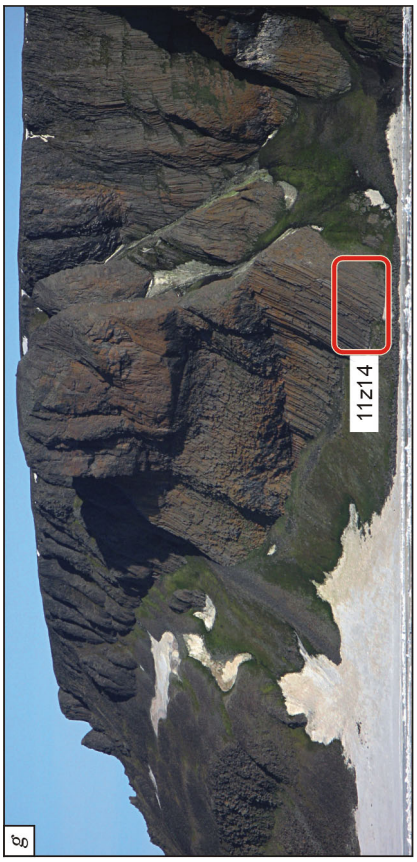

Fig. 6. Geologic aspects of the northern part of Hooker Island. *a*, geological framework: *1*, Jurassic–Early Cretaceous basalts and dolerites, non partitioned; *2*, Rubini Rock stock; *3*, paleomagnetic sampling sites with indication of their number; *4*, sampling sites for geochronological analysis with indication of age determinations; *b–g*, general view of the studied outcrops (Photographs by N. Mikhaltsov, M. Ivanov): lava flow dates in the bluff of Cape Sedov (*b*), volcanic section in Tikhaya Bay, east of Cape Sedov (*c*), Cape Albert Markham section (*d*), south of Cape Medvezhiy (*e*), Yuri Rock (*f*), Rubini Rock stock (*g*).

the initially less-ferruferrous titanomagnetite. At this, the time required for its transformation differs insignificantly from the time of the primary phase crystallization, and the same magnetization is measured in the newly formed high-ferriferous titanomagnetite as in the initially low-ferriferous grains (Pechersky and Didenko, 1995).

Studies of the low-temperature variation of magnetic susceptibility $k(T)$ have confirmed the presence of magnetite as the final oxidation phase of primary titanomagnetite and provided evidence of a "Verwey transition" (Verwey, 1939), occurring at a typical temperature of –153 °C, when a phase transition from cubic to orthorhombic magnetite occurs. However, in many samples, irreversible changes also take place in magnetite after heating, which results in discordance between the cooling and heating curves, while the repeated low-temperature curve does not exhibit the Verwey transition. The irreversible changes induced by laboratory heating were noticed in almost all the studied specimens, regardless of predominant magnetic phase, which implicitly indicates that after their formation, the rocks were not significantly affected by secondary heating and the resultant single-phase oxidation products can be considered as conventionally primary. The heating and cooling curves would otherwise be completely reversible.

The domain state of magnetic grains. The Day plot is concerned primarily with the size of the available magnetic grains. The larger these are, the closer their figurative points to the area corresponding to the multidomain state (MD field, Fig. 8), and the more badly the paleomagnetic signal is retained by the rock. The specimens studied are dominated by pseudo-single-domain (PSD) and marked by the presence of negligibly small single domain (SD) grains. At this, there is no correlation between a typical size of magnetic grains and the age of rocks.

Samples from lava flows of different age on Alexandra Land Island for example, are uniformly distributed along the lines of experimental values for magnetite, after (Dunlop, 2002), in the upper part of PSD field. There is no relationship observed either between the studied coercivity parameters and the morphological-textural variations or facies variety of rocks. A certain dependence can only be hinted based on the "territorial" approach.

For example, specimens from Ziegler Island, despite being represented by both dolerites of hypabyssal facies and typical lava basalts, form a single, distinctly discernible cluster in the upper part of the plot, i.e. have relatively low H_{cr}/H_c ratio values (where H_c is coercivity, H_{cr} is coercivity of remanence) and the maximum value of the M_{rs}/M_s ratio (where M_s is saturation magnetization, M_{rs} is saturation remanence), which characterizes both the SD and close to it PSD size of the present magnetic grains (Fig. 8).

The rock magnetic analysis results thus allow to infer that the studied FJL flood basalts are dominated by small grains of primary magmatic or single-phase-oxidized during cooling titanomagnetite rocks. Given that the rocks did not undergo any significant thermal impact after their formation, this rules out remagnetization of the products of ancient Early Jurassic

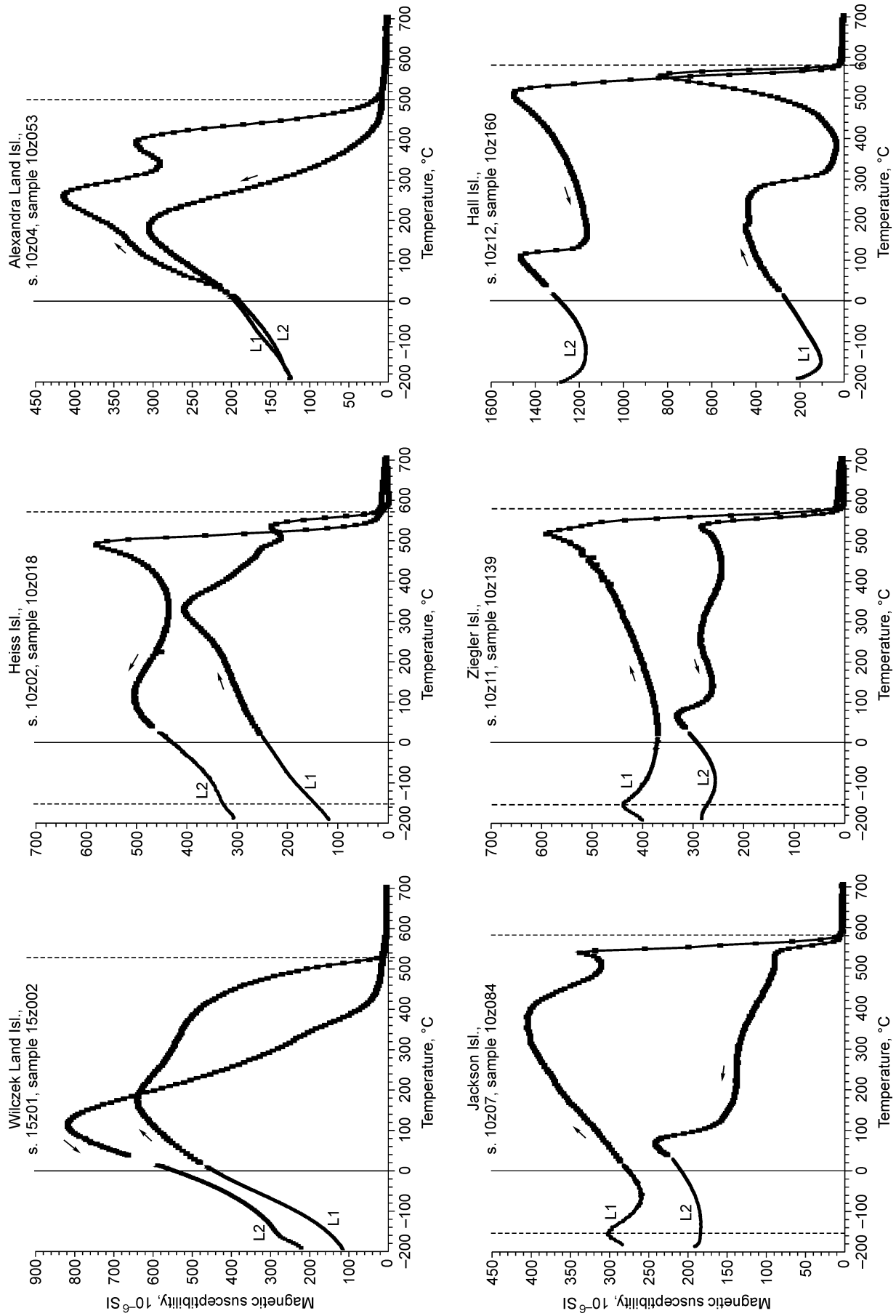

Fig. 7 (*continued on next page*).

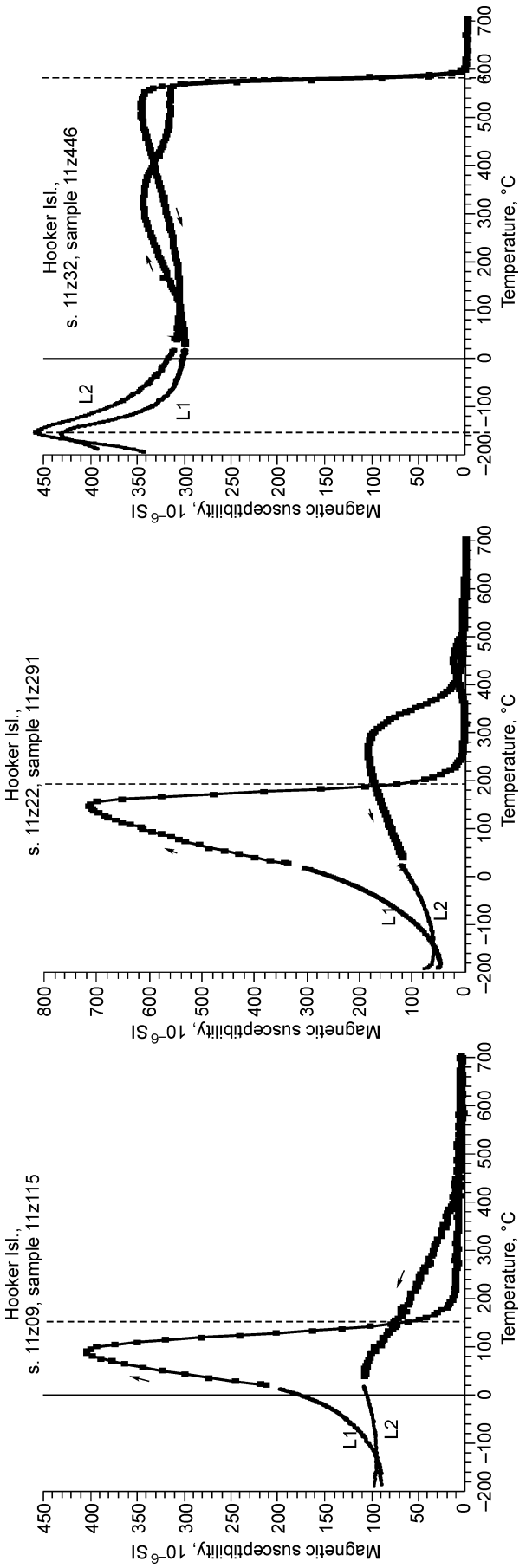

Fig. 7. Typical examples of magnetic susceptibility vs. temperature curves *k(T)* of the studied dolerites and basalts of Franz Josef Land. The arrows show heating (right) and cooling (left); L1 and L2, low-temperature curves before and after heating, respectively; dashed lines indicate the Curie curves-derived temperature for the present ferromagnetic minerals.

episode of magmatism associated with the heating during the following Late Jurassic and the most extensive Early Cretaceous events. This conclusion is best exemplified by the Alexandra Land Island section, where all the three above episodes of magmatism are expressed as consistently overlapping lava flows (Shipilov and Karyakin, 2014).

Component analysis. Results of AF-demagnetization have shown that, depending on the titanomagnetite composition in the specimen, the median destructive field (MDF) can vary from 5 to 50 mT, averaging, as a rule, about 20 mT (Fig. 9). Typically, first steps of demagnetization (<4–6 mT) induce the destruction of randomly oriented viscous magnetization formed after the sampling—during the specimens transportation, storage and preparation for research. However, it is difficult to estimate the contribution from the "natural" viscous component, formed *in situ* during the last period of positive geomagnetic polarity.

It probably degrades either simultaneously with the viscous magnetization formed in lab conditions or when affected by slightly higher-amplitude alternating magnetic field (AMF). Given that the geographical position of the FJL area since the time of the first magmatism pulse and during the late Mesozoic and Cenozoic corresponded high latitudes (near the true geomagnetic pole), it is difficult to differentiate between the viscous component direction and the primary Mesozoic one on the plots. As a result, characteristic remanent magnetization (ChRM) is destroyed almost in the entire AF-demagnetization interval or at least in the fields with the amplitude exceeding 14 mT and until the NRM disappears completely.

In as many as 60% of the samples magnetically hard, high ferriferous titanomagnetite or magnetite tend to be dominant, while AF-demagnetization is unable to destroy the NRM and isolate a stable component associated with these minerals. In this case, we used T-demagnetization. The destruction of the natural and lab-acquired viscous magnetization tends to occur already during the first heating to 150 °C. In most samples, the single expected ChRM is destroyed starting either from this point or when heated to ≈200 °C and up to the complete loss of natural magnetization at characteristic temperatures 540–600 °C (Fig. 9).

Sporadic presence of the intermediate component can be diagnosed in the samples in the range between 150 and 350 °C; its direction differs from that of ChRM by not more than 10°. The nature of this component, given the stable mineral composition of ferromagnetic minerals and the absence of evidence of chemical changes, appears evasive. It is most likely to be "false"—as an artifact emerging directly in the process of stepwise thermal demagnetization due to the interaction of the two determened ferrimagnetic phases of titanomagnetites with different unblocking temperatures (Shcherbakov et al., 2017).

Discussion and geological implications

The object-specific ChRM mean directions and their statistical parameters are given in Table 1, along with calculated

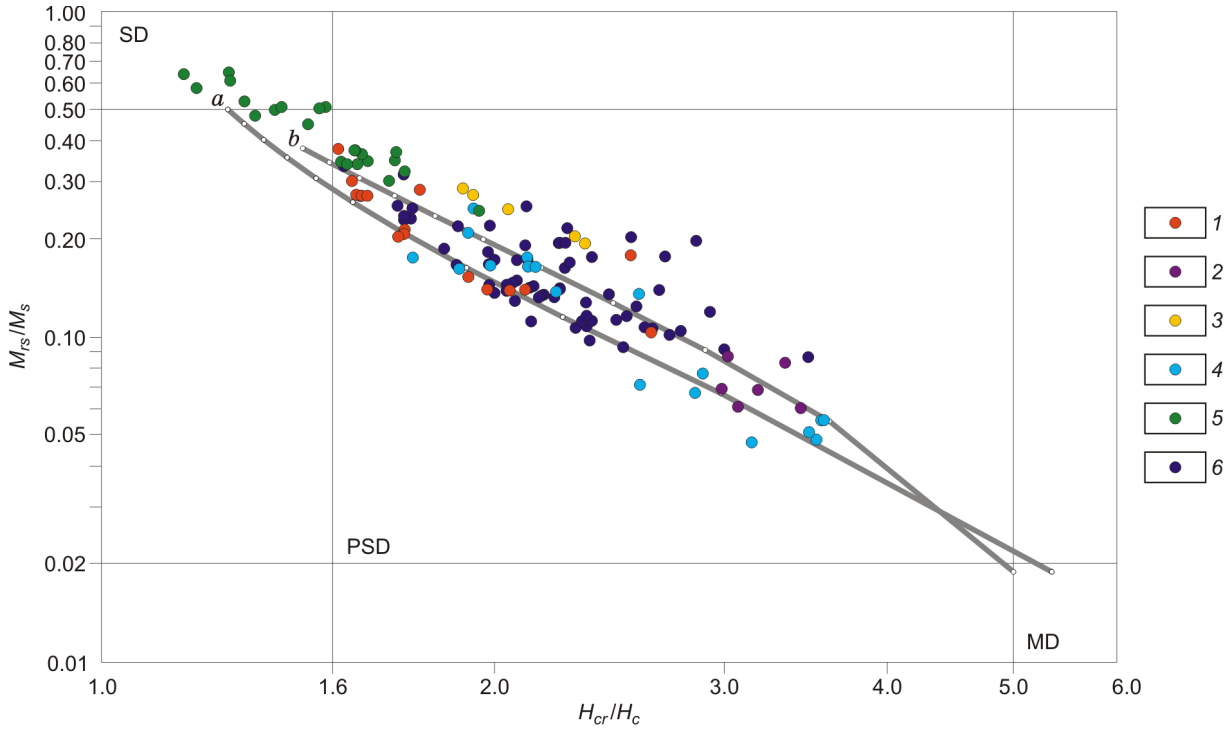

Fig. 8. Day plot from the FJL traps analysis: *1*, Alexandra Land Island; *2*, Hall Island; *3*, Jackson Island; *4*, Heiss Island; *5*, Ziegler Island; *6*, Hooker Island. The gray lines correspond to the experimental values for synthetic (*a*) and natural (*b*) magnetite (Dunlop, 2002). SD, Area of single-domain grains; PSD, area of pseudo-single domain grains; MD, area of multidomain grains.

coordinates for the corresponding virtual geomagnetic poles (VGPs). The discussed above rock magnetic aspects serve as the main arguments in favor of the primary nature of the established ChRMs: these are primarily the magmatic origin of the magnetization-carriers, the evidence of oxidation and changes in the composition of titanomagnetites that accounted only for the stage of rocks cooling and, finally, the absence of superimposed thermal events.

As is the case with our objects, standard field tests are of no use. Specifically, there are neither conglomerates in the structure of the studied part of the FJL trap section, nor overlying coarse clastic rocks, which would have allowed to conduct the conglomerate test. The most common fold test is also not applicable, since in this paper, we consider all paleomagnetic directions only in the modern (geographical) coordinate system, without introducing corrections for any possible changes in the primary spatial orientation of rocks relative to the paleohorizontal, as was done in the preliminary report (Mikhaltsov et al., 2016).

Unfortunately, in the absence of reliable observations, substantiation of the paleohorizontal at the time of trap magmatism is all but impossible. However, the investigated sloping surfaces of the top and base, or a systematic deviation from vertical columnar jointing, which were interpreted as a paleohorizontal (Mikhaltsov et al., 2016), are very likely to be reflective of the ancient topography and may have resulted from the lava flowing along the paleoslope.

Given that there is neither information about significant deformations in the trap section in the late Mesozoic–Cenozoic geological history of the FJL Archipelago area, nor obvious geologic evidence of possible inclinations of the studied lava flows and intrusions are available, while the rock magnetic data may imply the absence of large tectonothermal events, it would be methodically correct to use the geographic coordinate system in the established paleomagnetic directions distribution analysis, which means interpreting the position of the studied objects as undisturbed.

Finally, a reversal test cannot be properly used to substantiate the origin and age of established ChRMs either, since only one object (Ametistovaya dike on Heiss Island) has a reverse polarity. All other studied bodies are magnetized in the intervals of the direct (normal) polarity of the geomagnetic field (Table 1). The clear dominance of direct ChRM polarity appears strange, considering the supposed long history of magmatism from Early Jurassic to Early Cretaceous. All this time until the turn of the Barremian–Aptian, 126.3 Ma (Gradstein et al., 2012), the Earth's magnetic field was characterized by very frequent reversals, although normal polarity slightly predominated in general. It is only beginning from the Aptian and through the Santonian that the lengthy C34 superchron with normal polarity was recorded (Opdyke and Channel, 1996).

In this context, the data obtained mostly support the concept of a single brief magmatic event during the formation of the FJL province, and the time of this activity manifestation is closer to the second half of the Early Cretaceous. Nevertheless, the available $^{40}Ar/^{39}Ar$ ages, both Cretaceous and Jurassic, have shown a good correlation with the global Geomagnetic

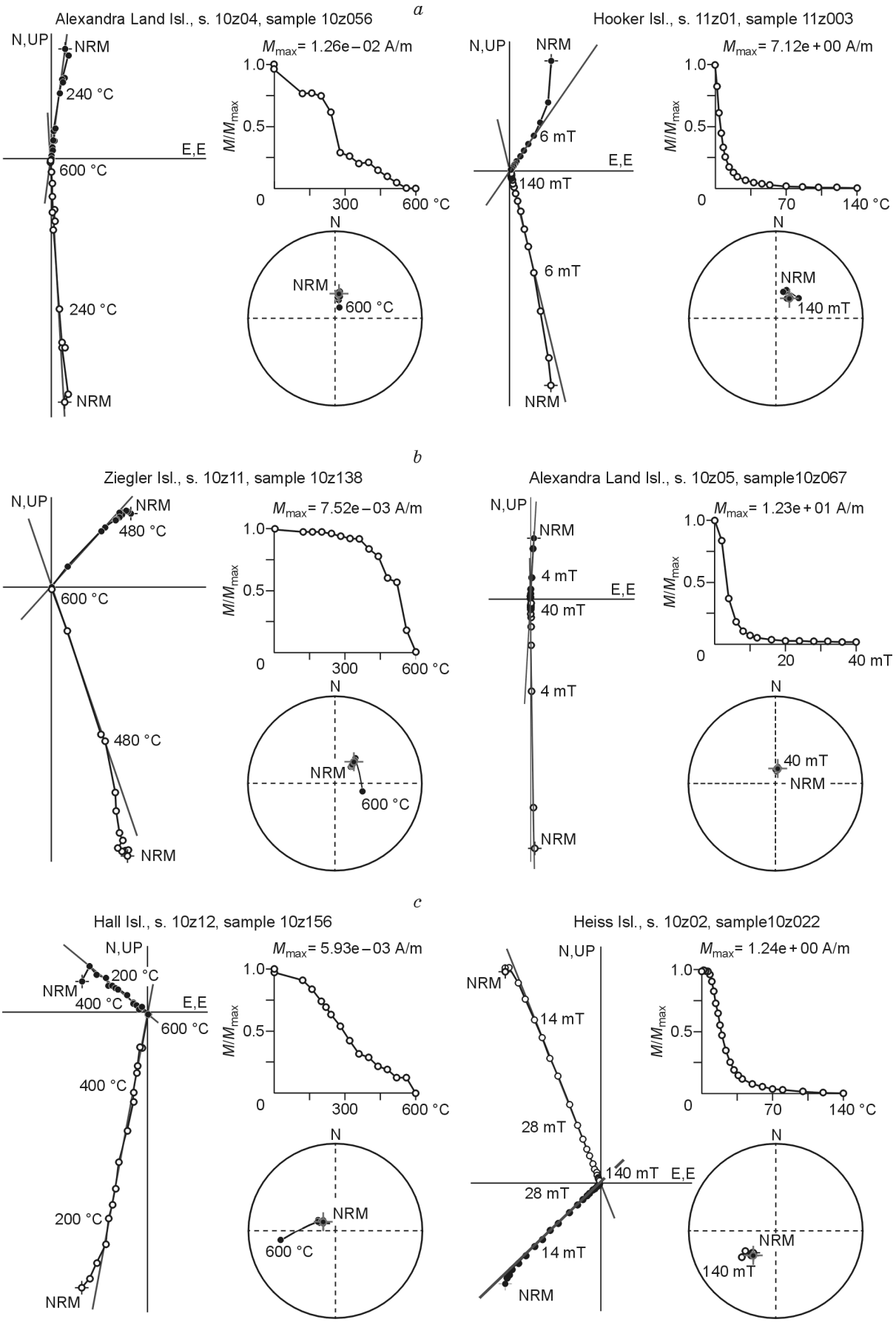

Fig. 9. Examples of *T*-demagnetization (left) and AF-demagnetization (right) of Early Jurassic (*a*); Late Jurassic (*b*) and Early Cretaceous (*b*) rocks of the FJL trap complex.

Table 1. Results of paleomagnetic analysis of the FJL traps

No.	Object of study (sampling site)	Glat	Glon	Age, Ma	*n/N*	*D*	*I*	*K*	α_{95}	Plat	Plon	A95	PL
Hall Island, east of Cape Wiggins													
1	Dike (10z12)*	80.4575	57.3773	132.3 ± 2.0	13/13	348.8	76.4	241.3	2.7	73.4	254.6	4.8	64.2
Wilczek Land Island, Cape Hanz													
2	Sill (15z01)	80.3842	59.7009	–	10/10	100.5	70.0	1036.8	1.5	51.2	127.1	2.4	53.9
Heiss Island, the E. Krenkel polar station area													
3	Ametistovaya dike (10z01,02)*	80.6126	57.8985	125.2 ± 5.5	19/23	222.7	–74.3	254.0	2.1	–66.8	0.6	3.6	–60.7
4	Lower sill (10z03)*	80.6202	58.0755	126.2 ± 2.8	8/8	6.2	76.4	118.9	5.1	73.5	228.6	9.1	64.2
5	Upper sill (10z13)*	80.6202	58.0755	132.0 ± 2.0	8/8	25.5	77.0	282.6	3.3	73.2	199.4	9.5	65.2
Ziegler Island, south of Cape Brice													
6	Lava flow-1 (10z09)*	81.0906	56.1076	136.8 ± 2.3	11/11	53.6	65.5	42.9	7.1	52.4	173.5	10.4	47.7
7	Lava flow-2 (10z10)	81.0903	56.1114	135.2 ± 6.3	13/13	58.5	53.2	253.4	2.6	38.0	171.9	3.0	33.8
8	Dike-1 (10z08)	81.0900	56.1006	126.0 ± 3.5	18/18	53.2	71.3	88.3	3.7	60.5	170.5	6.0	55.9
9	Dike-2 (10z11)	81.0906	56.1007	148.7 ± 4.2	12/12	46.1	69.9	151.6	3.5	59.4	179.4	5.6	53.8
Jackson Island, southern side of Cape Krensmuenster													
10	Lower sill (10z07)	81.2942	57.9327	123.9 ± 1.9	9/12	44.2	68.3	–	2.7	57.2	184.6	4.2	51.5
Alexandra Land Island, northern side of Severnaya Bay													
11	Lower lava flow (10z04)*	80.7725	47.6414	189.9 ± 3.1	31/33	7.1	71.2	197.1	1.8	64.9	218.2	2.9	55.8
12	Middle lava flow (10z05)*	80.7749	47.6249	156.5 ± 5.3	12/13	1.4	77.0	540.2	1.9	74.4	225.4	3.4	65.2
13	Upper lava flow (10z06)*	80.7749	47.6249	135.0 ± 4.0	5/5	349.6	83.1	129.8	6.7	85.2	258.0	13.0	76.4
Hooker Island, southwestern part of Sedov plateau (Cape Sedov and northern side of Tikhaya Bay)													
14	Lava flow on Cape Sedov, at the base of the Tikhaya Bay section (11z01,02)*	80.3407	52.7821	189.1 ± 11.4	27/27	33.4	68.7	214.6	1.9	59.7	190.6	3.0	52.1
15	Higher flow No. 14 (11z03)*	80.3395	52.8124	–	15/17	5.3	69.4	127.4	3.4	62.7	225.9	5.4	53.1
16	Lava flow, idem (11z05)*	80.3399	52.8004	–	25/27	68.6	74.0	153.2	2.3	62.3	146.9	3.9	60.2
17	Lava flow capping Cape Sedov (11z11)*	80.3434	52.7798	–	10/15	36.7	74.2	807.5	1.7	67.5	182.4	2.9	60.5
18	Lava flow capping Sedov Glacier (11z09)	80.3424	52.8858	–	10/10	27.1	78.0	171.3	3.7	74.9	189.6	6.8	67.0
19	Sill beneath lava flow No. 18 (11z10)	80.3422	52.8847	–	8/10	74.4	83.7	454.5	2.6	76.5	115.7	5.1	77.5
20	Sill, ibidem (11z08)	80.3427	52.8856	–	15/15	20.7	72.7	506.3	1.7	66.9	204.5	2.8	58.1
21	Sill, ibidem (11z07)	80.3454	52.9175	–	10/10	24.5	75.7	118.3	4.5	71.4	196.8	7.9	63.0
22	Sill, ibidem (11z06)	80.3455	52.9186	–	12/12	15.7	71.2	702.2	1.5	64.9	211.9	2.4	55.8
Hooker Island, central and northern parts of Sedov plateau													
23	Molchaniya valley, sill beneath the upper lava flow (11z12)	80.3527	52.8451	–	7/10	352.7	79.9	165.8	4.7	79.9	246.9	8.8	70.4
24	Molchaniya valley, upper lava flow (11z13)	80.3527	52.8448	–	15/16	41.6	72.7	201.4	2.7	64.6	178.0	4.5	58.1
25	Voronin Glacier, upper lava flow (11z25)	80.3597	52.8972	–	17/17	35.6	68.7	143.0	2.9	59.4	188.1	4.5	52.1

(*continued on next page*)

Table 1 (*continued*)

No.	Object of study (sampling site)	Glat	Glon	Age, Ma	*n*/*N*	*D*	*I*	*K*	α_{95}	Plat	Plon	A95	PL
Hooker Island, central and northern parts of Sedov plateau													
26	Cape Albert Markham, middle lava flow (11z18)	80.3889	53.0294	–	9/12	44.0	71.2	165.8	4.0	62.0	176.8	6.5	55.8
27	Cape Albert Markham, lower lava flow (11z19)	80.3889	53.0301	–	8/14	59.9	76.1	147.3	4.6	67.0	153.4	8.2	63.7
Hooker Island, southern side of Cape Medvezhiy													
28	Lower sill (11z20)	80.2714	52.6834	–	5/11	96.5	80.7	293.6	4.5	68.5	110.4	8.5	71.9
29	Upper sill (11z21)	80.2716	52.6830	–	12/12	30.4	70.0	76.8	5.0	62.0	193.4	8.0	53.9
30	Upper lava flow (11z22)	80.2718	52.6844	–	8/16	352.1	75.4	254.2	3.5	72.1	244.6	6.1	62.5
Hooker Island, central and eastern parts													
31	Pila cliff, lower lava flow (11z26)	80.3227	53.2473	–	11/14	72.6	82.7	309.1	2.6	75.3	122.5	5.0	75.6
32	Pila cliff, upper lava flow (11z24)	80.3223	53.1914	–	16/16	78.1	71.4	377.5	1.9	56.8	140.5	3.1	56.1
33	Solnechnaya Rock, lower lava flow (11z27)	80.3031	53.2430	–	16/16	15.3	69.3	177.6	2.6	62.2	213.3	4.1	52.9
34	Solnechnaya Rock, middle lava flow (11z28)	80.3027	53.2357	–	14/14	23.2	74.5	202.4	2.8	69.6	200.0	4.8	61.0
35	Solnechnaya Rock, upper lava flow (11z29)	80.3028	53.2260	–	10/12	15.5	78.6	278.3	2.9	77.1	206.6	5.3	68.0
36	Yuri Rock, lower lava flow (11z32)	80.2778	52.9821	–	6/6	48.9	67.2	165.8	4.7	55.7	173.7	7.1	49.9
37	Yuri Rock, middle lava flow (11z30)	80.2733	52.9993	–	9/13	49.8	60.4	23.3	10.9	47.1	175.5	14.4	41.4
38	Yuri Rock, upper lava flow (11z31)	80.2737	52.9981	–	16/16	42.5	71.4	152.2	2.9	62.5	178.1	4.7	56.1
Hooker Island, Rubini Rock													
39	Stock, facing north (11z14)	80.3386	52.7721	145 ± 7	10/17	99.4	79.6	1379.8	1.3	66.3	110.7	2.4	69.8
40	Stock, facing south (11z23)	80.3149	52.8241	145 ± 7	19/20	38.6	82.2	181.0	2.5	80.2	156.9	4.8	74.7
Scott-Keltie Island, eastern ending													
41	Lower lava flow (11z15)	80.3289	52.6288	–	15/15	60.5	68.8	120.3	3.5	56.1	159.8	5.5	52.2
42	Middle lava flow (11z16)	80.3287	52.6308	–	17/17	55.5	64.9	63.8	4.5	51.7	167.3	6.5	46.9
43	Upper lava flow (11z17)	80.3285	52.6272	–	10/15	35.2	76.4	320.9	2.7	71.3	181.1	4.8	64.2
Average values for FJL													
44	George Land Island **			130–100	12	30.0	82.0	120.0	2.0	81.2	165.6	3.8	74.3
45	VGP for objects with Early Cretaceous absolute ages			145–125	11	40.0	75.8	57.0	6.1	69.5	180.2	10.8	63.2
46	VGP for objects with Jurassic absolute ages			190–148	4	27.3	72.5	139.7	7.8	65.7	199.5	13.0	57.8
47	VGP for objects w/o absolute ages			–	28	43.4	75.3	83.5	3.0	68.2	176.7	5.2	62.3
48	All poles, except VGP for objects with Jurassic absolute ages			145–125	40	42.4	75.7	76.6	2.6	68.9	177.5	4.5	62.9

Note. Object numbering corresponds to numbers in Fig. 11; age—available $^{40}Ar/^{39}Ar$ and K/Ar data (the authors of determinations are referred to in the text); Glat and Glon are latitude (N) and longitude (E) of the sampling point (Nos. 45–48: the Champ Island coordinates are accepted as average values: 80.7, 56.0); *n*/*N* is ratio of number used in statistics to the total number of independently oriented samples (for averages—number of poles used in statistics); *D* and *I*, paleomagnetic declination and inclination; *K*, precision parameter; α_{95}, radius of 95% confidence circle for direction; Plat and Plon, the pole's latitude (N) and longitude (E); A95, radius of 95% confidence circle for pole; PL, paleolatitude for the object. All angular values and coordinates are given in degrees.

* Paleomagnetic data, after (Mikhaltsov et al., 2016).

** Paleomagnetic data, after (Gusev, 1970).

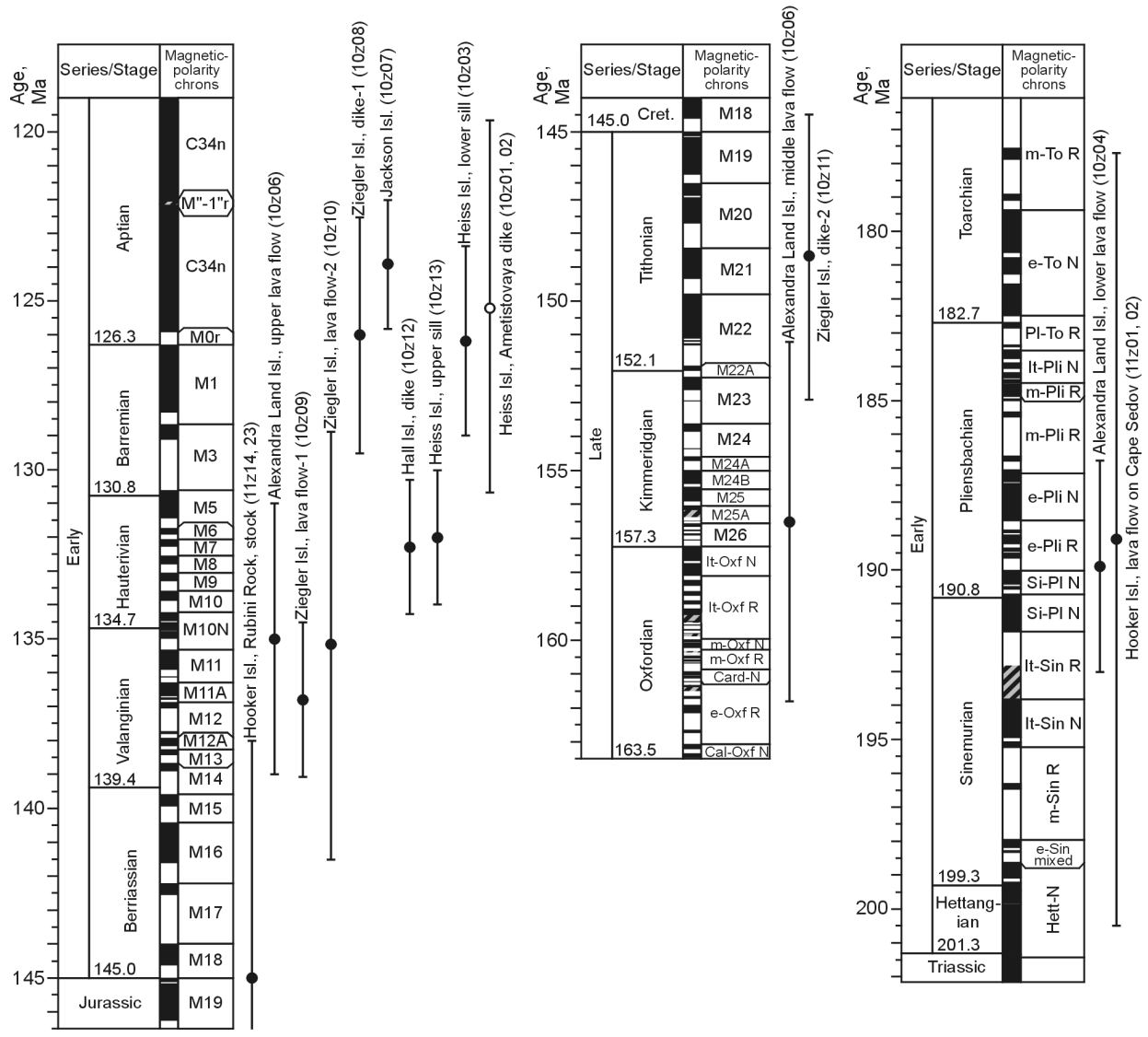

Fig. 10. Comparison of results of the FJL traps dating and polarity of isolated magnetization components with the Geomagnetic Polarity Time Scale (Gradstein et al., 2012). Black color is for the intervals of normal polarity, white—for reverse polarity, gray with black shading—for anomalous polarity; vertical segments—confidence intervals for the available absolute age determinations.

Polarity Time Scale (GPTS), and in some cases allow to more precisely define the intervals of events associated with the lava effusions and intrusions of dikes and sills (Fig. 10). These include the age from Ametistovaya dike 125.2 ± 2.0 Ma (Shipilov and Karyakin, 2014) showing very good agreement with GPTS, where the Aptian base exposes the narrow (125.9–126.3 Ma) M0r zone with reverse polarity (Gradstein et al., 2012). The age appears to be identical to the results of $^{40}Ar/^{39}Ar$ dating of the reverse-magnetized basalts of guyot MIT—125.4 ± 0.2 Ma, which serve as a basis for the M0r zone determination when deciphering the bands of magnetic anomalies in the Pacific Ocean (Pringle and Duncan, 1995).

The lower sill, which has a close $^{40}Ar/^{39}Ar$ age (126.2 ± 2.8 Ma) is located within the borders of that same Heiss Island where GhRM has a direct polarity, and corresponds to the M1n chron; its intrusion, according to the GPTS, shortly preceded the formation of Ametistovaya dike, in the range from 126.3 to 128.3 Ma (Fig. 10). The angle between the GhRM directions in these intrusions is 9.3°, its critical value being 4.4° according to the reversal test (McFadden and McElhinny, 1990).

The test, in itself, being a formal procedure, which yielded predictably negative result, can not be viewed as an argument against the inference about the paleomagnetic signal being recorded during the formation of intrusions. The determined ChRM directions reflect the "instantaneous" state of the geomagnetic field, from which it follows that secular variations have not been averaged and the compared poles are virtual geomagnetic poles (VGPs), and therefore not consistent with the central Axial Dipole Hypothesis, being a necessary condition for the reversal test performance (Butler, 1992).

A good correlation between the $^{40}Ar/^{39}Ar$ data (131.6 ± 2.4 Ma) and GPTS (M5n chron 130.6–131.4 Ma) is typical of the upper sill on Heiss Island and most others dated as

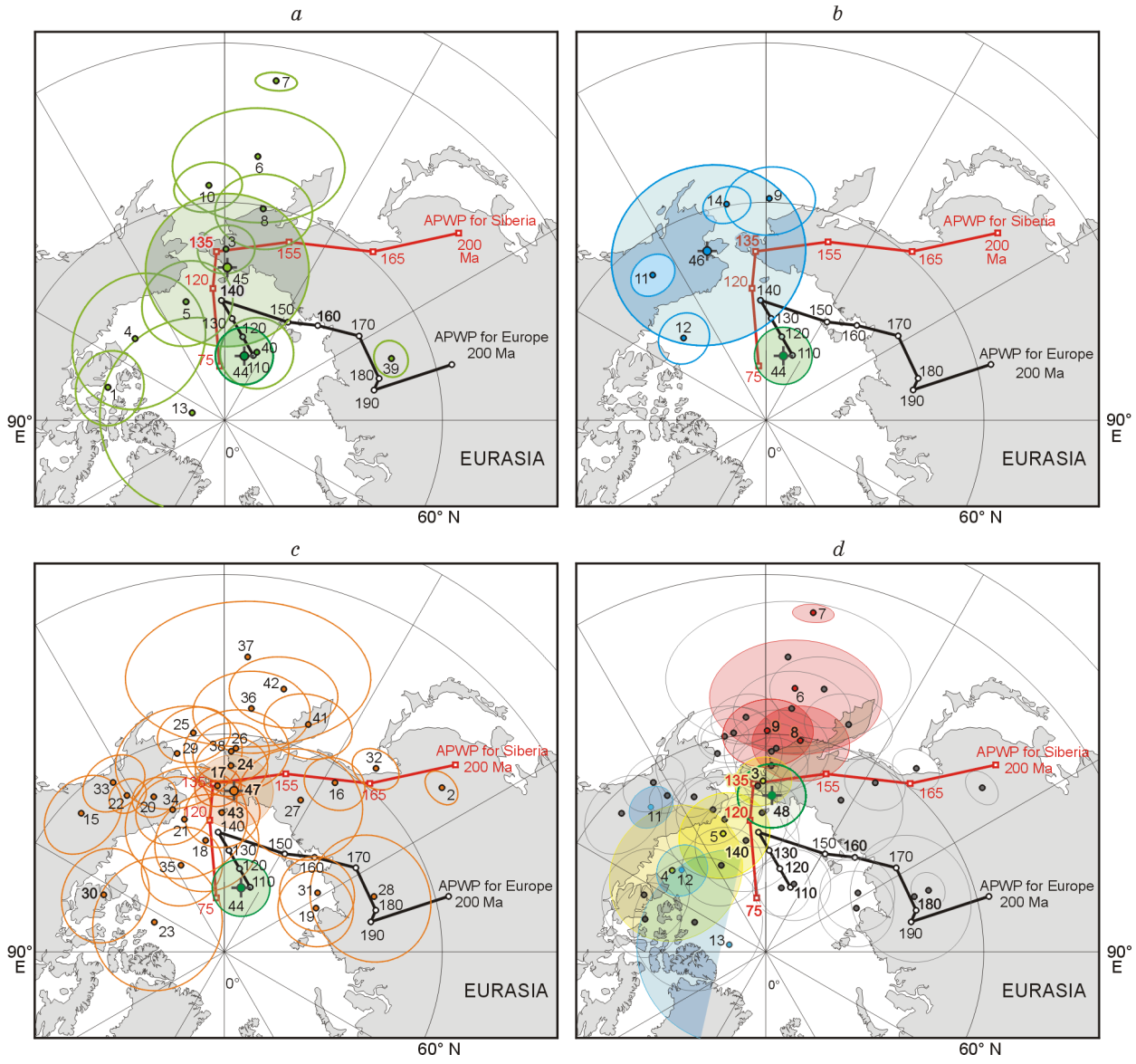

Fig. 11. Position of calculated VGPs and average paleomagnetic poles of the FJL traps as compared with Mesozoic APWP intervals for Europe (Torsvik et al., 2012) and Siberia (Metelkin et al., 2010): VGP with Early Cretaceous absolute age determinations of rocks (*a*); VGP with Jurassic absolute age determinations of rocks (*b*); VGP for objects without absolute age determinations of rocks (*c*); all available VGPs (*d*); marked red are VGPs for Ziegler Island, yellow—for Heiss Island, blue—for Alexandra Land Island. The numbers at the poles correspond to the pole order numbering in Table 1.

Early Cretaceous and Late Jurassic bodies, since all of them find adequate analogues in GPTS (Fig. 10). This to some extent supports the "randomness" in the normal polarity prevalence in our data set, as well as the episodic pattern and short duration of magmatism during the putative magmatic pulses.

Somewhat less well substantiated is the lack of reverse polarity in lava flows dated as the Sinemurian–Pliensbachian interval of the Early Jurassic. In our sampling, only two specimens have corresponding $^{40}Ar/^{39}Ar$ dates: the lower flow on Alexandra Land Island (189.9 ± 3.1 Ma) and lava flow on Hooker Island in the vicinity of Cape Sedov (189.1 ± 11.4 Ma). The available ages factoring the definition errors "overlap" a number of polarity chrons, with their average values being consistent with the prevailing reverse polarity epoch, which is referred to as the Early Pliensbachian e-Pli R chron on the GPTS (Fig. 10). The Early Jurassic interval of the GPTS is generally characterized by extreme frequency in reversals and, unlike the Late Jurassic–Early Cretaceous interval, has no corresponding confirmations from ocean magnetic anomalies and is calibrated on the scale of biostratigraphic units (Gradstein et al., 2012). Most of the chrons are therefore differentiated by the predominant polarity, and may comprise up to ten narrow zones with opposite sign (geomagnetic reversals). Among them, the Early Pliensbachian chron with predominantly reverse polarity includes at least 6 (!) normal polarity zones (Gradstein et al., 2012). Therefore, given such a small data set and $^{40}Ar/^{39}Ar$ measurement

accuracy, the presence of direct polarity ChRM alone is not surprising.

One of the paleomagnetic reliability criteria consists in the concidence between the obtained paleomagnetic determinations with the data independently obtained by other authors (van der Voo, 1990). Before the commencement of our work, the Global Paleomagnetic Database (IAGA GPDB) contained only one determination in the FJL traps, for the supposedly Early Cretaceous basalts of George Land Island (Gusev, 1970).

Even though the investigations were conducted back in the 60s of the last century, the author managed to get a result that meets most of the modern criteria of reliability of paleomagnetic data. The statistics was derived from a set of 42 specimens collected from 12 lava flows that total 180 m in thickness, which suggests averaging of secular variations, whereas the absence of remagnetization is corroborated by the conglomerate test (Gusev, 1970). The basalts age, in itself, is not sufficiently substantiated according to the modern standards. Nevertheless, we use this determination in our further analysis along with the data obtained, assuming, after the author, that it is part of the Early Cretaceous episode of magmatic activity (Table 1).

All of the calculated VGPs (virtual geomagnetic poles) form a scattered cloud centered in the area of modern Chukotka (Fig. 11). That said, it is problematic to segregate anticipated discrete groups with predominance of VGPs of knowingly different ages. The two Early Jurassic and two Late Jurassic VGPs whose age is determined from $^{40}Ar/^{39}Ar$ analysis, as well as the more abundant Early Cretaceous poles, are completely indistinguishable within the total body of data and concentrated near the Early Cretaceous interval of the apparent polar wander paths (APWP) for Europe (Torsvik et al., 2012) and Siberia (Metelkin et al., 2010), while being more consistent with the latter (Fig. 11).

For the purpose of comparative analysis a different variant of Siberia's APWP, which is based on more rigid principles of the actual data selection can be used (Didenko, 2015). As such, the Early Cretaceous segments of these APWPs differ only in detail and bear no fundamental contradictions in respect of the substantiation of the Franz Josef Land magmatism evolution. The available set of dated VGPs corresponding to the Early Cretaceous pulse of magmatic activity appears sufficient for averaging secular variations, while the mean pole will correspond to the 145–125 Ma paleomagnetic pole in the context of the geocentric axial dipole hypothesis.

The pole's coordinates (Plat = 69.5, Plong = 180.2, A95 = 10.8, N = 11) do not differ significantly from the paleomagnetic pole obtained earlier from the George Land Island basalts (Table 1, Fig. 11*a*). The angular distance is 11.5 ± 7.9. The new pole coordinates for the Early Cretaceous episode of magmatism, when compared with the average pole for all objects with Jurassic $^{40}Ar/^{39}Ar$ dates Plat = 65.7, Plong = 199.5, A95 = 13.0, N = 4 (Fig. 11*b*), indicate that the difference of 7.7 ± 11.1 is statistically insignificant. There are also no differences, when the same pole is compared with the rest of the data set Plat = 68.2, Plong = 176.7, A95 = 5.2, N = 28 (Fig. 11*c*), angular distance: 1.8 ± 8.8. At first glance, all this appears indicative of a singular magmatism event on the FJL Archipelago, disagreeing the obtained Jurassic $^{40}Ar/^{39}Ar$ dates. However, a more detailed analysis shows that this conclusion is premature.

In the analyzed data set, the VGPs of Early Cretaceous episode of magmatic activity confidently predominate. Either the vast majority or, possibly, all of the objects of this paleomagnetic analysis undated by the isotope method may also correspond to this time. VGPs exhibit obvious significant variability (Fig. 11), which can be explained only by the geomagnetic field variations against the backdrop of frequent reversals. This effect is enhanced by the high-latitude position of the FJL province which persisted throughout the late Mesozoic and Cenozoic (Dobretsov et al., 2013; Gaina et al., 2014; Shipilov and Vernikovsky, 2010). It has been proved that the VGP variance which is associated with secular variations of the earth's magnetic field, is directly proportional to the object's latitudinal position during the fixation of magnetization and it tends to increase almost two-fold at the poles, as compared to the equator (Merrill and McElhinny, 1983). This means that the coincidence of individual Jurassic VGPs with an Early Cretaceous paleomagnetic pole is simply explained by a lack of the statistics data in the context of high-latitude variance caused by secular variations in the epoch of frequent polarity reversals.

It thus appears impossible to characterize either the paleomagnetic pole or the FJL trap province position at the Early and Late Jurassic stages of its evolution, nor to substantiate these magmatism episodes with the available set of paleomagnetic data. However, there is every indication that the Early Cretaceous pole (145–125 Ma) Plat = 68.9, Plong = 177.5, A95 = 4.5, N = 40 calculated for the entire data sample with the exception of the four poles that have Jurassic $^{40}Ar/^{39}Ar$ dates, is underpinned by sufficient factual materials and can be used for paleotectonic reconstructions. This is confirmed by angular dispersion (S) calculations which serves as the standard for quality evaluation of averaging the secular variations (McFadden, 1980). In our case, S = 15.9°, which differs little from hypothetical value of $S = 19°$ for the 62.9° E latitude, at which, according to the data obtained, the FJL trap province was located in the Early Cretaceous, and fully meets the model condition for correct averaging of secular variations: $10° < S < 20°$ (Merrill and McElhinny, 1983).

The obtained paleomagnetic pole with account of estimation error coincides with the corresponding age interval (140–120 Ma) of the APWP for Siberia, which is statistically different from that of the coeval APWP interval for Europe (Fig. 11). Within the existing tectonic representations, the differences between the Mesozoic intervals of Siberian and European APWPs are explained by intraplate strike-slip tectonics (Metelkin et al., 2008, 2010, 2012). In this case, the correlation between the Early Cretaceous pole of the FJL province and the APWP for Siberia suggests a possibility of coeval shear deformations in this part of the Svalbard plate with the Siberian domain. The geological manifestations of this process may be either strike-slips inherited from the late Paleozoic–early Mesozoic structural transformations of the

Paykhoy–Novaya Zemlya region (Abashev et al., 2017; Bogdanov et al., 1997), or those associated with the formative processes for the Canadian basin (Shipilov, 2016) and later processes of the Arctic Ocean evolution.

Lastly, there is another specific feature of the calculated VGPs distribution. Given the comparison and data sample analysis were made separately for the islands, it is remarkable that they have a certain tendency for grouping. For example, the positions of VGP for Ziegler, Heiss, and Alexandra Land Islands have a quite compact disposition (Fig. 11*d*). In part, this trend may be associated with low-amplitude local displacements during the formation of the present day terrain, although no pronounced deformations that could have caused these displacements can be identified. Another possible cause is the presence of several magmatism centers during the formation of the entire Barents Sea LIP and the FJL uplift structure, in particular. In this case, the observed pattern may reflect site-specific features of the magmatism of these centers. However, regardless of their representations, the discussed variations tend to be leveled off, since the statistics involves determinations for several such groups, while the average and paleomagnetic poles are fully consistent.

Conclusions

The conducted paleomagnetic studies attest to the preservation of magnetization produced by the FJL traps formation. However, a significant variance in VGPs positions, due to the high-latitude position of the Barents Sea LIP and secular variations at the time period characterized by frequent geomagnetic reversals that preceded the onset of the Cretaceous C34 superchron, does not allow to identify the anticipated discrete groups of poles that would correspond to brief pulses of magmatism activation in the Early and Late Jurassic and Early Cretaceous, as is suggested by contemporary $^{40}Ar/^{39}Ar$ data (Dobretsov et al., 2013; Karyakin and Shipilov, 2009; Shipilov, 2016). On the contrary, the available set of paleomagnetic and isotope-geochronological data provides evidence in favor of total dominance of the products of the Early Cretaceous (145–125 Ma) episode of magmatism. Alternatively, the hypothesis of episodic magmatism during the formation of the Barents Sea LIP and the presence of the Jurassic stage in magmatic activity on the FJL Archipelago cannot be completely disregarded based on the obtained paleomagnetic data largely due is the inability to take into account secular variations, given the insignificant statistics for VGP of presumably Jurassic age. In other words, even supposing that the Jurassic magmatism pulses exist, the close positions of Jurassic and Early Cretaceous paleomagnetic poles and significant variations in the Earth's magnetic field, the corresponding VGPs distributions become significantly overlapped. It is therefore impossible to divide them using statistical methods alone, without involving additional independent petrological-geochemical, isotope-geochronological or other geological-geophysical criteria.

Given that all parameters of the Early Cretaceous paleomagnetic pole calculated from the analysis results satisfy the central axial dipole hypothesis, it can characterize the position of the Franz Josef Land Archipelago and the Barents Sea LIP during this, probably main stage of magmatic activity. With account of confidence ellipse, the Early Cretaceous pole of Franz Josef Land does not differ from the corresponding APWP interval for Siberia. At the same time, the Mesozoic part of the Siberian APWP exhibits systematic differences from European APWP, which is explained by mutual sinistral strike-slips within the Eurasian continent derived from existing tectonic models. Their occurrence is associated with the lagging effect in the European tectonic domain during the general clockwise rotation of the Eurasian plate, with the domain center (Euler pole) corresponding to the inner part of the Siberian craton (Metelkin et al., 2008, 2010, 2012). Within the framework of these reconstructions, the coincidence of paleomagnetic data for the FJL territory with the Siberian APWP rather than the European one, may imply the involvement of the studied part of the Svalbard plate in the discussed intraplate movements at the side of the Siberian tectonic domain. It can be assumed that the reconstructed intracontinental motions in the region are associated with the kinematics of the opening of the Arctic Ocean and reflect the global tectonics process.

Acknowledgments. The authors express their sincere gratitude to Yu.V. Karyakin (Geological Institute, Russian Academy of Sciences, Moscow) for scientific advice and invaluable assistance in organizing and conducting the 2010–2011 fieldwork on the Franz Josef Land Archipelago. The authors also thank the Lomonosov Northern (Arctic) Federal University, the Russian Artic National Park, the crew of the "Professor Molchanov" research vessel for their assistance in the 2017 Expedition to Franz Joseph Land for additional investigations within the Arctic Floating University's innovative educational project. The authors also would like to thank A.N. Vasilevsky (IPGG SB RAS, Novosibirsk), A.A. Kartoziya (IGM SB RAS, Novosibirsk) for their help in processing and interpretation of the published geophysical and bathymetry data, and N.Yu. Matushkin for correcting the English text of the paper.

The work was supported by the Russian Science Foundation, RSF (Project 14-37-00030), the Russian Foundation for Basic Research (Projects 16-05-00523, 16-05-00888, 18-35-00273) and the RF Ministry of Education and Science (Projects 5.2324.2017/4.6, 5.4786.2017/6.7).

References

Abashev, V.V., Metelkin, D.V., Mikhal'tsov, N.E., Vernikovsky, V.A., Matushkin, N.Yu., 2017. Paleomagnetism of the Upper Paleozoic of the Novaya Zemlya Archipelago. Izvestiya, Physics of the Solid Earth 53 (5), 677–694.

Andersen, O.B., Knudsen, P., Kenyon, S., Factor, J.K., Holmes, S., 2017. Global gravity field from recent satellites (DTU15)—Arctic improvements. First Break 35, No. 12, 37–40.

Bogdanov, N.A., Khain, V.E., Shipilov, E.V., 1997. Early Mesozoic geodynamics of the Barents–Kara region. Dokl. Akad. Nauk 357 (2), 511–515.

Buchan, K.L., Ernst, R.E., 2006. Giant dike swarms and reconstruction of the Canadian Arctic islands, Geenland, Svalbard and Franz Josef Land, in: Hanski, E., Mertanen, S., Rämö, T., Vuollo, J. (Eds.), Dike Swarms: Time Markers of Crustal Evolution. Tailor & Francis/Balkema, Amsterdam, pp. 27–48.

Butler, R.F., 1992. Paleomagnetism: Magnetic Domains to Geologic Terranes. Blackwell.

Corfu, F., Polteau, S., Planke, S., Faleide, J.I., Svensen, H., Zayoncheck, A., Stolbov, N., 2013. U–Pb geochronology of Cretaceous magmatism on Svalbard and Franz Josef Land, Barents Sea Large Igneous Province. Geol. Mag. 150 (6), 1127–1135.

Day, R., Fuller, M., Schidt, V.A., 1977. Hysteresis properties of titanomagnetites: Grain size and compositional dependence. Phys. Earth Planet. Inter. 13, 260–267.

Didenko, A.N., 2015. The analysis of Meso-Cenozoic paleomagnetic poles and apparent polar wander path of Siberia. Fizika Zemli, No. 5, 65–79.

Dobretsov, N.L., 2010. Global geodynamic evolution of the Earth and global geodynamic models. Russian Geology and Geophysics (Geologiya i Geofizika) 51 (6), 592–610 (761–784).

Dobretsov, N.L., Vernikovsky, V.A., Karyakin, Yu.V., Korago, E.A., Simonov, V.A., 2013. Mesozoic–Cenozoic volcanism and geodynamic events in the Central and Eastern Arctic. Russian Geology and Geophysics (Geologiya i Geofizika) 54 (8), 874–887 (1126–1144).

Dunlop, D.J., 2002. Theory and application of the Day plot (Mrs/Ms versus Hcr/Hc) 1. Theoretical curves and tests using titanomagnetite data. J. Geophys. Res. 107, B3, EPM 4-1–EPM 4-22.

Enkin, R.J., 1994. A computer program package for analysis and presentation of paleomagnetic data. Pacific Geoscience Centre, Geological Survey of Canada.

Ernst, R.E., 2014. Large Igneous Provinces. Cambridge University Press.

Evenchick, C.A., Davis, W.J., Bedard, J.H., Hayward, N., Friedman, R.M., 2015. Evidence for protracted High Arctic large igneous province magmatism in the central Sverdrup Basin from stratigraphy, geochronology, and paleodepths of saucer-shaped sills. GSA Bull. 127 (9/10), 1366–1390.

Filatova, N.I., Khain, V.E., 2009. Structural units of the Central Arctic and their relation to the Mesozoic Arctic plume. Geotektonika, No. 6, 24–51.

Gaina, C., Medvedev, S., Torsvik, T.H., Koulakov, I., Stephanie, C., 2014. Werner 4D Arctic: A Glimpse into the Structure and Evolution of the Arctic in the Light of New Geophysical Maps, Plate Tectonics and Tomographic Models. Surv. Geophys. 35, 1095–1122, doi: 10.1007/s10712-013-9254-y.

Grachev, A.F., 2001. A new view on the origin of magmatism of the Franz Joseph Land. Fizika Zemli, No. 9, 49–61.

Gradstein, F.M., Ogg, J.G., Schmitz, M.D., Ogg, G.M., 2012. The Geological Time Scale. Elsevier.

Gusev, B.V., 1970. Trap magnetism of the Franz Joseph Land Archipelago compared with North Siberian trap magnetism, in: Proc. 8th Conf. Constant Geogeomagnetic Field and Paleomagnetism [in Russian]. Naukova Dumka, Kiev, Part 1, pp. 55–58.

Ivanov, A.V., He, H., Yan, L., Ryabov, V.V., Shevko, A.Y., Palesskii, S.V., Nikolaeva, I.V., 2013. Siberian Traps large igneous province: evidence for two flood basalt pulses around the Permo–Triassic boundary and in the Middle Triassic, and contemporaneous granitic magmatism. Earth. Sci. Rev. 122, 58–76.

Jowitt, S.M., Williamson, M.-C., Ernst, R.E., 2014. Geochemistry of the 130 to 80 Ma Canadian High Arctic Large Igneous Province (HALIP) event and implication for Ni–Co–PGE prospectivity. Econ. Geol. 109, 281–307.

Kamo, S.L., Czamanske, G.K., Amelin, Yu., Fedorenko, V.A., Davis, D.W., Trofimov, V.R., 2003. Rapid eruption of Siberian flood-volcanic rocks and evidence for coincidence with the Permian–Triassic boundary and mass extinction at 251 Ma. Earth Planet. Sci. Lett. 214 (1–2), 75–91.

Karyakin, Yu.V., Shipilov, E.V., 2009. Geochemical specifics and $^{40}Ar/^{39}Ar$-age of the basaltoid magmatism of the Alexandra Land, Northbrook, Hooker, and Hayes islands (Franz Josef Land Archipelago). Dokl. Earth Sci. 425 (2), 260–263.

Kazanskii, A.Yu., Kazanskii, Yu.P., Saraev, S.V., Moskvin, V.I., 2000 The Permo-Triassic boundary in volcanosedimentary section of the West Siberian plate according to paleomagnetic data (*from studies of the core of the Tymenskaya superdeep borehole SDB-6*). Geologiya i Geofizika (Russian Geology and Geophysics) 41 (3), 327–339 (323–335).

Kazansky, A.Yu., Metelkin, D.V., Bragin, V.Yu., Kungurtsev, L.V., 2005. Paleomagnetism of the Permian–Triassic traps from the Kuznetsk Basin, southern Siberia. Russian Geology and Geophysics (Geologiya i Geofizika) 46 (11), 1089–1102 (1107–1120).

Kirschvink, J.L., 1980. The least squares line and plane and analysis of paleomagnetic data. Geophys. J. Roy. Astron. Soc. 62, 699–718.

Koulakov, I.Yu., Gaina, K., Dobretsov, N.L., Vasilevsky, A.N., Bushenkova, N.A., 2013. Plate reconstructions in the Arctic region based on joint analysis of gravity, magnetic, and seismic anomalies. Russian Geology and Geophysics (Geologiya i Geofizika) 54 (8), 859–873 (1108–1125).

Kremenetsky, A.A., Kostitsin, Yu.A., Morozov, A.F., Rekant, P.V., 2015. Sources of the magmatic rocks of the Mendeleev Rise, Arctic Ocean: evidence from isotope-geochemical data. Geokhimiya, No. 6, 487–501.

Kuzmin, M.I., Yarmolyuk, V.V., 2014. Mantle plumes of Central Asia (Northeast Asia) and their role in forming endogenous deposits. Russian Geology and Geophysics (Geologiya i Geofizika) 55 (2), 120–143 (153–184).

Kuzmin, M.I., Yarmolyuk, V.V., 2016. Plate tectonics and mantle plumes as a basis of deep-seated Earth's tectonic activity for the last 2 Ga. Russian Geology and Geophysics (Geologiya i Geofizika) 57 (1), 8–21 (11–30).

Kuzmin, M.I., Yarmolyuk, V.V., Kravchinsky, V.A., 2010. Phanerozoic hot spot traces and paleogeographic reconstructions of the Siberian continent based on interaction with the African large low shear velocity province. Earth Sci. Rev. 102 (1–2), 29–59.

Kuzmin, M.I., Yarmolyuk, V.V., Kravchinsky, V.A., 2011. Phanerozoic Within-Plate Magmatism of North Asia: Absolute Paleogeographic Reconstructions of the African Large Low-Shear-Velocity Province. Geotektonika 45 (6), 3–23.

Latyshev, A.V., Veselovsky, R.V., Ivanov, A.V., Fetisova, A.M., Pavlov, V.E., 2013. Evidence of brief intense peaks of magmatic activity in the south Siberian platform (Angara–Taseeva Basin) as indicated bypaleomagnetic studies. Fizika Zemli, No. 6, 77–90.

Laverov, N.P., Lobkovsky, L.I., Kononov, M.V., Dobretsov, N.L., Vernikovsky, V.A., Sokolov, S.D., Shipilov, E.V., 2013. The Mesozoic and Cenozoic history of the Arctic: A geodynamic model and a problem of shelf outer boundary. Geotektonika, (1), 1–32 .

Lawver, L.A., Grantz, A., Gahagan, L.M. 2002. Plate kinematic evolution of the present Arctic region since the Ordovician. Geol. Soc. Am. Bull., Spec. Pap. 360, 337–362.

McFadden, P.L., 1980. Testing a paleomagnetic study for the averaging of secular variation. Geophys. J. Res. 61, 183–192.

McFadden, P.L., McElhinny, M.W., 1990. Classification of the reversal test in paleomagnetism. Geophys. J. Int. 103, 725–729.

Merrill, R.T., McElhinny, M.W., 1983. The Earth's magnetic field: Its History, Origin and Planetary Perspective. Acad. Press, London.

Metelkin, D.V., Vernikovsky, V.A., Kazansky, A.Yu., Kashirtsev, V.A., Bragin, V.Yu., Kungurtsev, L.V., 2008. The Mesozoic apparent polar wander path for the Siberian domain of the Eurasian plate. Dokl. Earth Sci. 418 (4), 62–67.

Metelkin, D.V., Vernikovsky, V.A., Kazansky, A.Yu., Wingate, M.T.D., 2010. Late Mesozoic tectonics of Central Asia based on paleomagnetic evidence. Gondwana Res. 18 (2–3), 400–419.

Metelkin, D.V., Vernikovsky, V.A., Kazansky, A.Yu., 2012. Tectonic evolution of the Siberian paleocontinent from the Neoproterozoic to Late Mesozoic: paleomagnetic record and reconstructions. Russian Geology and Geophysics (Geologiya i Geofizika) 53 (7), 675–688 (883–899).

Mikhaltsov, N.E., Kazansky, A.Yu., Ryabov, V.V., Shevko, A.Ya., Kuprish, O.V., Bragin, V.Yu., 2012. Paleomagnetism of trap basalts in the northwestern Siberian craton, from core data. Russian Geology and Geophysics (Geologiya i Geofizika) 53 (11), 1228–1242 (1595–1613).

Mikhaltsov, N.E., Karyakin, Yu.V., Abashev, V.V., Bragin, V.Yu., Vernikovsky, V.A., Travin, A.V., 2016. Geodynamics of the Barents–Kara margin in the Mesozoic inferred from paleomagnetic data on rocks from the Franz Joseph Land Archipelago. Dokl. Earth Sci. 471, 1242–1246.

Minakov, A., Faleide, J.I., Glebovsky, V.Yu., Mjelde, R., 2012. Structure and evolution of the northern Barents–Kara Sea continental margin from

integrated analysis of potential fields, bathymetry and sparse seismic data. Geophys. J. Int. 188, 79–102.

Morozov, A.F., Petrov, O.V., Shokalsky, S.P., Kashubin, S.N., Kremenetsky, A.A., Shkatov, M.Yu., Kaminsky, V.D., Gusev, E.A., Grikurov, G.E., Rekant, P.V., Shevchenko, S.S., Sergeev, S.A., Shatov, V.V., 2013. New geological data confirming continental origin of the Central Arctic Rises. Regionalnaya Geologiya i Metallogeniya 53, 34–55.

Nagata, T., 1961. Rock Magnetism. Maruzen Company LTD, Tokyo.

Ntaflos, Th., Richter, W., 2003. Geochemical constraints on the origin of the continental Flood Basalt magmatism in Franz Josef Land, Arctic Russia. Eur. J. Miner. 15 (4), 649–663.

Opdike, N.D., Channel, J.E.T., 1996. Magnetic Stratigraphy. Academ. Press, New York.

Pechersky, D.M., Didenko, A.N., 1995. Paleo-Asian Ocean: Rock Magnetic and Paleomagnetic Information Concerning Its Lithosphere [in Russian]. OIFZ RAN, Moscow.

Piskarev, A.L., Heunemann, K., Makariev, A.A., Makarieva, E.M., Bakhtadze, V., Aleksyutin, M., 2009. Magnetic parameters and compositions of igneous rocks in the Franz Josef Land Archipelago. Izv. RAN, Fizika Zemli, No. 2, 66–83.

Pringle, M.S., Duncan, R.A., 1995. Radiometric ages of basaltic lavas recovered at Lo-En, Wodejebato, MIT, and Takuyo-Daisan Guyots, northwestern Pacific Ocean. Proc. Ocean Drilling Program, Scientific Results 144, 547–557.

Reichow, M.K., Pringle,, M.S., Al'Mukhamedov A.I., Allen, M.B., Andreichev, V.L., Buslov, M.M., Davies,, C., Fedoseev G.S., Fitton, J.G., Inger, S., Medvedev, A.Ya., Mitchell, C., Puchkov, V.N., Safonova, I.Yu., Scott, R.A., Saunders, A.D., 2009. The Timing and Extent of the Eruption of the Siberian Traps Large Igneous Province: Implications for the End-Permian Environmental Crisis. Earth Planet. Sci. Lett. 277 (1–2), 9–20.

Shcherbakov, V.P., Latyshev, A.V., Veselovsky, R.V., Tselmovich, V.A., 2017. Origin of false components of NMR during conventional stepwise thermal demagnetization. Russian Geology and Geophysics (Geologiya i Geofizika) 58 (9), 1118–1128 (1407–1421).

Shipilov, E.V., 2011. Late Mesozoic volcanism of the East-Arctic continental margin of Eurasia (East Siberian Sea) based on seismic data. Dokl. Earth Sci. 436 (2), 181–185.

Shipilov, E.V., 2016. Basaltic magmatism and strike-slip tectonics in the Arctic margin of Eurasia: evidence for the early stage of geodynamic evolution of the Amerasia Basin. Russian Geology and Geophysics (Geologiya i Geofizika) 57 (12), 1668–1687 (2115–2142).

Shipilov, E.V., Karyakin, Yu.V., 2010. New data on basaltoid magmatism of western Spitzbergen. Dokl. Earth Sci. 430 (2), 252–257.

Shipilov, E.V., Karyakin, Yu.V., 2011. The Barent Sea magmatic province: Geological-geophysical evidence and new Ar^{39}/Ar^{40} ages. Dokl. Earth Sci. 439 (1), 955–960.

Shipilov, E.V., Karyakin, Yu.V., 2014. Dikes of Hayes Island (Franz Joseph Land Archipelago): tectonic position and geodynamic interpretation. Dokl. Earth Sci. 457 (1), 814–818.

Shipilov, E.V., Lobkovskii, L.I., 2014. The submeridional strike-slip zone in the structure of the Chukchi Sea continental margin and the mechanism of opening of Canada oceanic basin. Dokl. Earth Sci. 455 (1), 238–242.

Shipilov, E.V., Vernikovsky, V.A., 2010. The Svalbard–Kara plates junction: structure and geodynamic history. Russian Geology and Geophysics (Geologiya i Geofizika) 51 (1), 58–71 (75–92).

Shipilov, E.V., Karyakin, Yu.V., Matishov, G.G., 2009. Jurassic–Cretaceous Barents–Amerasian superplume and initial stage of geodynamic evolution of the Arctic Ocean. Dokl. Earth Sci. 426 (4), 564–573.

Sklyarov, E.V., Karyakin, Yu.V., Karmanov, N.S., Tolstykh, N.D., 2016. Platinum group minerals in dolerites of the Alexandra Land Island (Franz Josef Archipelago). Russian Geology and Geophysics (Geologiya i Geofizika) 57 (5), 834–841 (1058–1067).

Sokolov, S.D., Tuchkova, M.I., Ganelin, A.V., Bondarenko, G.E., Layer, P.W., 2015. Tectonism of the South-Anyui suture (NE Asia). Geotektonika, No. 1, 5–30.

State Geological Map of the Russian Federation. Scale: 1:1,000,000 (New Series), 2006. Sheet U-37-40, Franz Joseph Land [in Russian]. VSEGEI, St. Petersburg.

Stolbov, N.M., 2005. The Franz Joseph Land Archipelago as a Key Geological Marker of the Barents Sea Continental Margin. Extended Abstract of Cand. Sci. (Geol.-Miner.) Dissertation. St. Petersburg.

Stolbov, N.M., Suvorova, E.B., 2010. The age of the Franz Josef Land flood basalts, from geological evidence, in: The Nature of Shelf and Archipelagoes of the European Arctic [in Russian]. GEOS, Moscow, Issue 10, pp. 276–280.

Tarakhovsky, A.N., Fishman, M.V., Shkola, I.V., Andreichev, V.L, 1982. The age of traps of the Franz Josef Land. Dokl. Akad. Nauk SSSR 266 (4), 965–969.

Torsvik, T.H., Smethurst, M.A., 1999. Plate tectonic modelling: virtual reality with GMAP. Comput. Geosci. 25, 395–402.

Torsvik, T.H., Van der Voo, R., Preeden, U., Mac Niocaill, C., Steinberger, B., Doubrovine, P.V., van Hinsbergen, D.J.J., Domeier, M., Gaina, C., Tohver, E., Meert, J.G., McCausland, P.J.A., Cocks, L.R.M., 2012. Phanerozoic polar wander, paleogeography and dynamics. Earth Sci. Rev. 114, 325–368.

van der Voo, R., 1990. The reliability of paleomagnetic data. Tectonophysics 184, 1–9.

Vernikovsky, V.A., Dobretsov, N.L., Metelkin, D.V., Matushkin, N.I., Koulakov, I.Yu., 2013. Concerning tectonics and the tectonic evolution of the Arctic. Russian Geology and Geophysics (Geologiya i Geofizika) 54 (8), 838–858 (1083–1107).

Verwey, E.J.W., 1939. Electron conduction of magnetite (Fe_3O_4) and its transition point at low temperatures. Nature 144, 327–328.

Editorial responsibility: N.L. Dobretsov